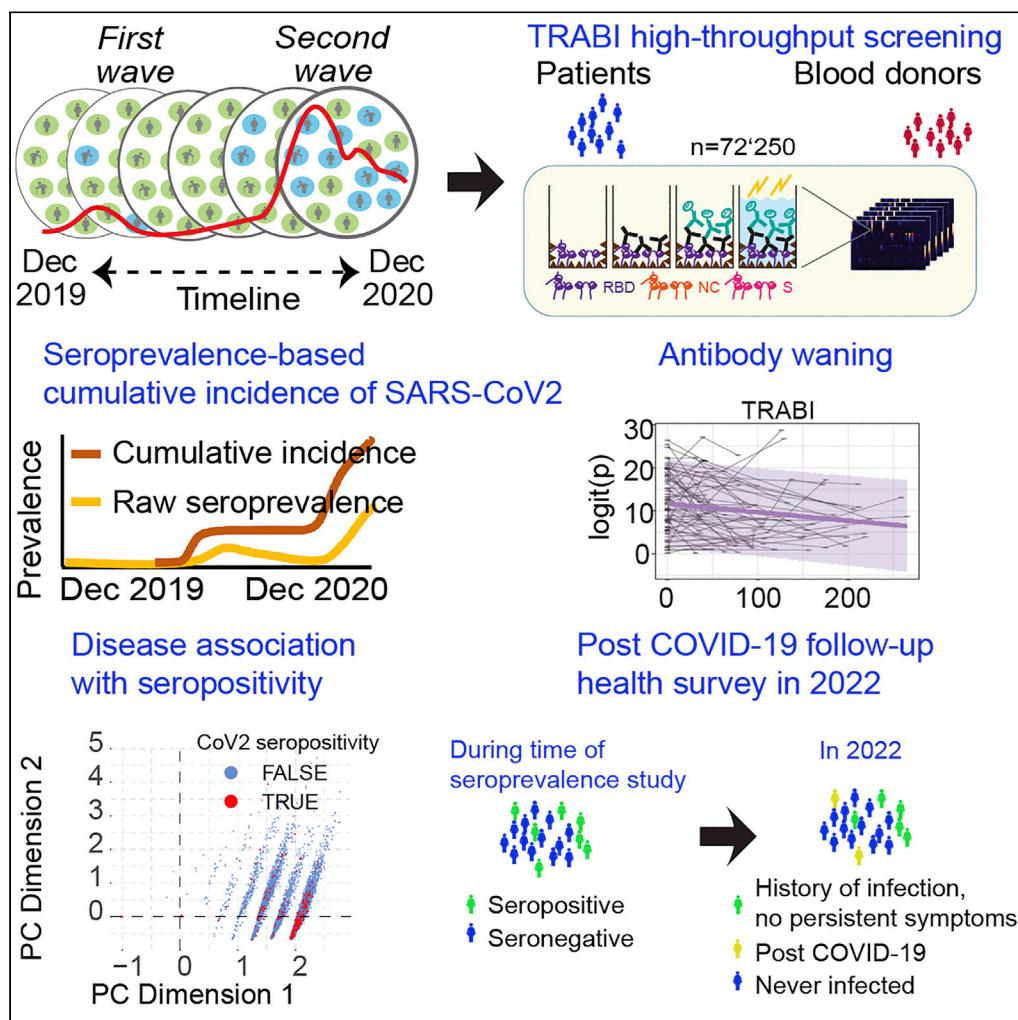


Article

Continuous population-level monitoring of SARS-CoV-2 seroprevalence in a large European metropolitan region



Marc Emmenegger, Elena De Cecco, David Lamparter, ..., Ioannis Xenarios, David I. Stuart, Adriano Aguzzi

marc.emmenegger@usz.ch (M.E.)
adriano.aguzzi@usz.ch (A.A.)

Highlights

We continuously assessed SARS-CoV-2 seroprevalence in two cohorts (n = 72'250).

Modeled cumulative incidence was 3 × higher than suggested by PCR-based testing

On the population level, antibody half-life was 75 days

10% of individuals maintained symptoms one year post-COVID-19

Article

Continuous population-level monitoring of SARS-CoV-2 seroprevalence in a large European metropolitan region

Marc Emmenegger,^{1,28,*} Elena De Cecco,¹ David Lamparter,^{2,27} Raphaël P.B. Jacquat,^{3,4,27} Julien Riou,⁵ Dominik Menges,⁶ Tala Ballouz,⁶ Daniel Ebner,⁷ Matthias M. Schneider,³ Itzel Condado Morales,¹ Berre Doğançay,¹ Jingjing Guo,¹ Anne Wiedmer,¹ Julie Domange,¹ Marigona Imeri,¹ Rita Moos,¹ Chryssa Zografou,¹ Leyla Batkitar,¹ Lidia Madrigal,¹ Dezirae Schneider,¹ Chiara Trevisan,¹ Andres Gonzalez-Guerra,¹ Alessandra Carrella,¹ Irina L. Dubach,⁸ Catherine K. Xu,³ Georg Meisl,³ Vasilis Kosmoliaptsis,^{9,10} Tomas Malinauskas,¹¹ Nicola Burgess-Brown,¹² Ray Owens,^{11,13} Stephanie Hatch,⁷ Juthathip Mongkolsapaya,¹⁴ Gavin R. Screaton,¹⁴ Katharina Schubert,¹⁵ John D. Huck,¹⁶ Feimei Liu,¹⁶ Florence Pojer,¹⁷ Kelvin Lau,¹⁷ David Hacker,¹⁷ Elsbeth Probst-Müller,¹⁸ Carlo Cervia,¹⁸ Jakob Nilsson,¹⁸ Onur Boyman,^{18,19} Lanja Saleh,²⁰ Katharina Spanaus,²⁰ Arnold von Eckardstein,²⁰ Dominik J. Schaer,⁸ Nenad Ban,¹⁵ Ching-Ju Tsai,²¹ Jacopo Marino,²¹ Gebhard F.X. Schertler,^{21,22} Nadine Ebert,^{23,24} Volker Thiel,^{23,24} Jochen Gottschalk,²⁵ Beat M. Frey,²⁵ Regina R. Reimann,¹ Simone Hornemann,¹ Aaron M. Ring,¹⁶ Tuomas P.J. Knowles,^{3,4} Milo A. Puhon,⁶ Christian L. Althaus,⁵ Ioannis Xenarios,^{2,26} David I. Stuart,¹¹ and Adriano Aguzzi^{1,*}

SUMMARY

Effective public health measures against SARS-CoV-2 require granular knowledge of population-level immune responses. We developed a Tripartite Automated Blood Immunoassay (TRABI) to assess the IgG response against three SARS-CoV-2 proteins. We used TRABI for continuous seromonitoring of hospital patients and blood donors (n = 72'250) in the canton of Zurich from December 2019 to December 2020 (pre-vaccine period). We found that antibodies waned with a half-life of 75 days, whereas the cumulative incidence rose from 2.3% in June 2020 to 12.2% in mid-December 2020. A follow-up health survey indicated that about 10% of patients infected with wildtype SARS-CoV-2 sustained some symptoms at least twelve months post COVID-19. Crucially, we found no evidence of a difference in long-term complications between those whose infection was symptomatic and those with asymptomatic acute infection. The cohort of asymptomatic SARS-CoV-2-infected subjects represents a resource for the study of chronic and possibly unexpected sequelae.

INTRODUCTION

The severe acute respiratory syndrome coronavirus 2 (SARS-CoV-2, henceforth abbreviated as CoV2) is responsible for COVID-19^{2,3} and has caused millions of deaths. It has also indirectly caused many more fatalities by hijacking healthcare resources, thereby making them unavailable to patients suffering from other diseases. In addition, COVID-19 has created profound economic distress for most travel-related industries and has disrupted a plethora of industrial supply chains, resulting in a massive worldwide economic crisis that may cost many more human lives.

The canton of Zurich, with a population of approximately 1.5 million inhabitants, registered its first two COVID-19 cases on February 27, 2020. Zurich has seen a relatively mild first wave, with 134 deaths (and 3'785 reported cases) until June 31, 2020. However, the case numbers exploded in October, resulting in 460 deaths (and 45'516 reported cases) by December 1, 2020,⁴ with hospitals working at capacity limit. In order to alleviate the direct consequences of the CoV2 pandemic, governments and public healthcare agencies need granular and reliable data on the prevalence of infection, the incidence of new infections, and the spatial-temporal oscillations of these parameters within regions of interest.

¹Institute of Neuropathology, University of Zurich, 8091 Zurich, Switzerland

²Health2030 Genome Center, 9 Chemin des Mines, 1202 Geneva, Switzerland

³Centre for Misfolding Diseases, Department of Chemistry, University of Cambridge, Lensfield Road, Cambridge CB2 1EW, UK

⁴Cavendish Laboratory, Department of Physics, University of Cambridge, JJ Thomson Avenue, Cambridge CB3 0HE, UK

⁵Institute of Social and Preventive Medicine, University of Bern, 3012 Bern, Switzerland

⁶Epidemiology, Biostatistics and Prevention Institute, University of Zurich, Zurich, Switzerland

⁷Target Discovery Institute, University of Oxford, Oxford OX3 7FZ, England

⁸Division of Internal Medicine, University Hospital Zurich, 8091 Zurich, Switzerland

⁹Department of Surgery, Addenbrooke's Hospital, University of Cambridge, Hills Road, Cambridge CB2 0QQ, UK

¹⁰NIHR Blood and Transplant Research Unit in Organ

Continued



Intuitively, PCR-based diagnostics would seem suitable to fulfill the above criteria. However, practical experience has shown that this is not the case. The acquisition of representative diagnostic material for PCR has proven challenging, with deep nasal swabs being difficult to perform, uncomfortable for patients, and potentially hazardous for medical personnel. Accordingly, the sensitivity of PCR diagnostics is often disappointing, with reported false-negative rates of 25% even under the best conditions.⁵

Serological assays, on the other hand, address the adaptive immune responses of the host which are fundamental to limiting viral spread within individuals and populations. While they lag behind viral infection, they can serve as both powerful epidemiological tools as well as useful clinical aids. Firstly, antibodies can be easily retrieved from many biological fluids, notably venous and capillary blood. Secondly, antibodies typically persist for several months whereas the viral load in the upper respiratory tract frequently wanes within weeks.⁶ Importantly, immunological assays can be largely automated, and are thus suitable for mass screening of extremely large cohorts.

Although large serological surveys have been carried out in several countries,^{7–11} there is a lack of continuous seroprevalence data. As waning of CoV2 antibodies has been reported in multiple instances,^{12–16} single timepoint serology estimates may yield misleading insights into the true extent of CoV2 spread. We, therefore, aimed to investigate the evolution of the CoV2 seroprevalence in the canton of Zurich, a particularly low prevalence setting during the first and second waves in 2020, using an in-house developed tripartite automated blood immunoassay (TRABI) already employed in multiple studies.^{17–21} Continuous immunosurveys were conducted in a large cohort of the University Hospital of Zurich (n = 55'814 samples) and blood donors from the Blood Donation Services of the canton of Zurich (n = 16'291), over a period from December 2019 to December 2020, i.e. prior to the onset of the vaccination campaigns. Apart from assessing the underlying cumulative incidence, we aimed to build a foundation for the subsequent identification of sequelae in clinically well-characterized hospital patients. To this end, we have made use of available ICD-10 codes and free-text reports to elucidate whether seropositivity is associated with disease entities beyond those already reported. Finally, we invited serologically tested hospital patients to participate in an online health survey to investigate the follow-up health status of seropositive patients post-COVID-19, with the first infection dating back more than 500 days (median). These combined seroepidemiological and nosophidemiological endeavors, together with the close monitoring of ongoing vaccination efforts and variants of concerns (VOCs), are likely pivotal in enhancing our understanding of how to manage the current as well as future pandemic outbreaks.

RESULTS

Tripartite automated blood immunoassay: A miniaturized high-throughput enzyme-linked immunosorbent assay for multiple CoV2 antigens

Here we assessed the changes in CoV2 seroprevalence in the population of the canton of Zurich (n = 1.5 million) between December 2019 and December 2020. To this end, we developed a tripartite automated blood immunoassay (TRABI) utilizing contactless acoustic dispensing^{22,23} to transfer diluted plasma droplets (2.5 nL) into high-density 1536-well plates (total volume: 3 μ L) and measuring the IgG response against viral proteins by immunocolorimetry (Figures 1A and S1A for detailed procedure).

In order to identify the most suitable viral targets for TRABI, we infected Vero cells with wild-type CoV2 virus. Cell lysates were then subjected to Western blotting using the plasma of patients with confirmed COVID-19 (n = 7). The bands corresponding to the S and NC proteins were prominently visible in infected cells, but were undetectable in non-infected cells and were suppressed by adding soluble S and NC antigens to the patient plasma before incubation with the Western blot (Figure 1B). Accordingly, we selected the CoV2 spike protein,²⁴ the receptor binding domain (RBD, amino acids 330–532 of the S protein), and the nucleocapsid protein (NC, amino acids 1–419) as target antigens for TRABI. Each sample was tested at eight consecutive 2-fold dilution points (1:50 to 1:6'000), and the resulting data were fitted to a sigmoidal curve by logistic regression. The inflection point (or $-\log_{10}(\text{EC}_{50})$) of each sigmoid was defined as the respective antibody titer.

As reference samples for assay establishment, we utilized a collective of 55 venous plasma samples drawn at various days post onset of symptoms (dpo) from 27 RT-qPCR confirmed patients suffering from COVID-19 and hospitalized at the University Hospital of Zurich (USZ, true positives, see Tables 1 and S1), as well as 90 anonymized USZ samples from the prepandemic era (true negatives). We then constructed receiver operating

Donation and Transplantation, University of Cambridge, Hills Road, Cambridge CB2 0QQ, UK

¹¹Division of Structural Biology, The Wellcome Centre for Human Genetics, University of Oxford, Headington, Oxford OX3 7BN, UK

¹²Structural Genomics Consortium, University of Oxford, Oxford OX3 7DQ, UK

¹³The Rosalind Franklin Institute, Harwell Campus, Oxford OX11 0FA, UK

¹⁴Nuffield Department of Medicine, Wellcome Trust Centre for Human Genetics, University of Oxford, Oxford, UK

¹⁵Department of Biology, Institute of Molecular Biology and Biophysics, ETH Zurich, Zurich, Switzerland

¹⁶Department of Immunobiology, Yale School of Medicine, New Haven, CT, USA

¹⁷Protein Production and Structure Core Facility, EPFL SV PTECH PTPSP, 1015 Lausanne, Switzerland

¹⁸Department of Immunology, University Hospital Zurich, 8091 Zurich, Switzerland

¹⁹Faculty of Medicine, University of Zurich, 8006 Zurich, Switzerland

²⁰Institute of Clinical Chemistry, University Hospital Zurich, 8091 Zurich, Switzerland

²¹Department of Biology and Chemistry, Laboratory of Biomolecular Research, Paul Scherrer Institute, 5303 Villigen-PSI, Switzerland

²²Department of Biology, ETH Zürich, 8093 Zürich, Switzerland

²³Institute of Virology and Immunology, 3012 Bern, Switzerland

²⁴Department of Infectious Diseases and Pathobiology, Vetsuisse Faculty, University of Bern, 3012 Bern, Switzerland

²⁵Regional Blood Transfusion Service Zurich, Swiss Red Cross, 8952 Schlieren, Switzerland

²⁶Agora Center, University of Lausanne, 25 Avenue du Bugnon, 1005 Lausanne, Switzerland

Continued

characteristics (ROC) curves to assess the assay quality for each antigen individually. Finally, we created a composite metric that integrates S/RBD/NC measurements using quadratic discriminant analysis (QDA). While each single antigen showed excellent discrimination of negatives and positives on samples drawn at ≥ 14 dpo, the compound models outperformed the individual antigen measurements at 7–13 dpo, where the emergence of an IgG response is expected to be variable (Figure 1C, upper panel). We, therefore, used the QDA modeling assumptions to infer the prevalence in large cohorts based on the distributional information of true negatives and true positives using information gained from all three antigens.

To benchmark TRABI, we compared the results with a high-throughput assay—at the time of testing still under development—at the University of Oxford as well as assays commercialized by Roche (Elecsys), DiaSorin, EuroImmun, and Abbott (Figure 1C, lower panel). This comparative assessment was based on 136 of 146 samples (10 samples were removed from the analysis because of insufficient sample volume to perform all tests). While all assays displayed 100% specificity/sensitivity at late time points, TRABI scored best at early time points, also when additionally compared to a lateral-flow assay (Figure S2). When these results were plotted as a function of dpo, a temporal pattern emerged consistent with the gradual emergence of IgG antibodies within 14 dpo (Figure 1D).

Characterization of cohort used for seroprevalence estimates from December 2019 to December 2020

Anti-CoV2 antibodies were measured with TRABI in 66'630 copandemic samples (collected between December 2019 and December 2020), 51'435 belonging to patients of the USZ, and 15'195 to blood donors. On average, we collected and analyzed 3'957 (SD1'801) and 1'169 (SD273) samples per month, for USZ and BDS, respectively (Table 1). These samples were assigned to 48'561 individuals. 38'526 individuals (79.3%) provided one sample, 5'604 individuals (11.5%) two samples, 2'406 individuals (5.0%) three samples, and 2'025 individuals (4.2%) four or more samples; however, maximally one donation per month per individual was entering our pipeline. The median age of the USZ patients was 55 (40–68) years (Table 1 and Figure S3A) and 42 (28–54) years of the blood donors (Table 1 and Figure S3B), which was stable over the time span of our measurements for the USZ patients (Figure S3C) but showed deviations for the blood donors, with a decrease in overall age between April and August 2020, followed by an increase in age from henceforth (Figure S3D). The sex distribution in the USZ sample was stable over time, with a female/male ratio close to parity (Figure S3E). The BDS sample contained slightly more men than expected (Figure S3F). Most of the hospital patients included in this study were adult residents of the canton of Zurich (Figure S4A) and were treated in one of the many clinical departments (Figure S4B), the highest number in Medical Oncology and Hematology, followed by Cardiology, Infectious Diseases and Hospital Hygiene, Rheumatology, and Gastroenterology and Hepatology. The distribution of samples originating from these hospital wards was relatively stable over time (Figure S4C). 5'345 distinct ICD-10 codes were assigned to hospital patients, of which the 50 most common ones are summarized in Table S2. Within these 50 ICD-10 codes are many of the common diseases like 'essential primary hypertension' (ICD-10: I10.00), 'type II diabetes mellitus' (ICD-10: E11.9), or 'heart failure' (ICD-10: I50) but also 'chronic kidney disease' (ICD-10: N18), and 'malignant melanoma of skin' (ICD-10: C43).

Temporal evolution of the CoV2 epidemic in the greater area of Zurich

5'475 prepandemic samples collected before December 2019 were used as condition negatives (see Table 1) and 154 copandemic ($n = 78$ from USZ, $n = 76$ from BDS, see later in discussion) samples, included in the screen in the same manner as all other copandemic samples, identified as condition positives. Their annotation as condition positives was performed post-hoc using USZ and BDS databases in the absence of serological data. First, we identified all USZ samples with known positive CoV2 RT-qPCR results ($n = 320$). Condition-positive samples ($n = 78$) were defined as those with (1) clinically manifest COVID-19 pneumonia and (2) positive RT-qPCR for CoV2 and (3) venipuncture occurring ≥ 14 days after the positive qPCR to account for seroconversion. To avail of condition positives from the cohort of blood donors, 76 samples from convalescent individuals with PCR-confirmed CoV2 infection recruited for a plasmapheresis study conducted with blood donors and part of the same pool of BDS samples sent to us for the seroprevalence study were included—these samples were annotated as convalescent individuals post-hoc and were not used to estimate seroprevalence as they were study-specifically recruited by BDS, unlike all other blood donors whose blood was collected during routine blood donation and was then analyzed in our study. In addition to the QDA-based model that assumes that both the condition-positive and negative data follow distinct multivariate Gaussian distribution with unequal covariances (Figures 2A and 2B), we tested a model based on Gaussian distributions with equal covariances: linear discriminant analysis (LDA) (Figures S5A and S5B).

²⁷These authors contributed equally

²⁸Lead contact

*Correspondence:
marc.emmenegger@usz.ch
(M.E.),
adriano.aguzzi@usz.ch (A.A.)
<https://doi.org/10.1016/j.isci.2023.105928>

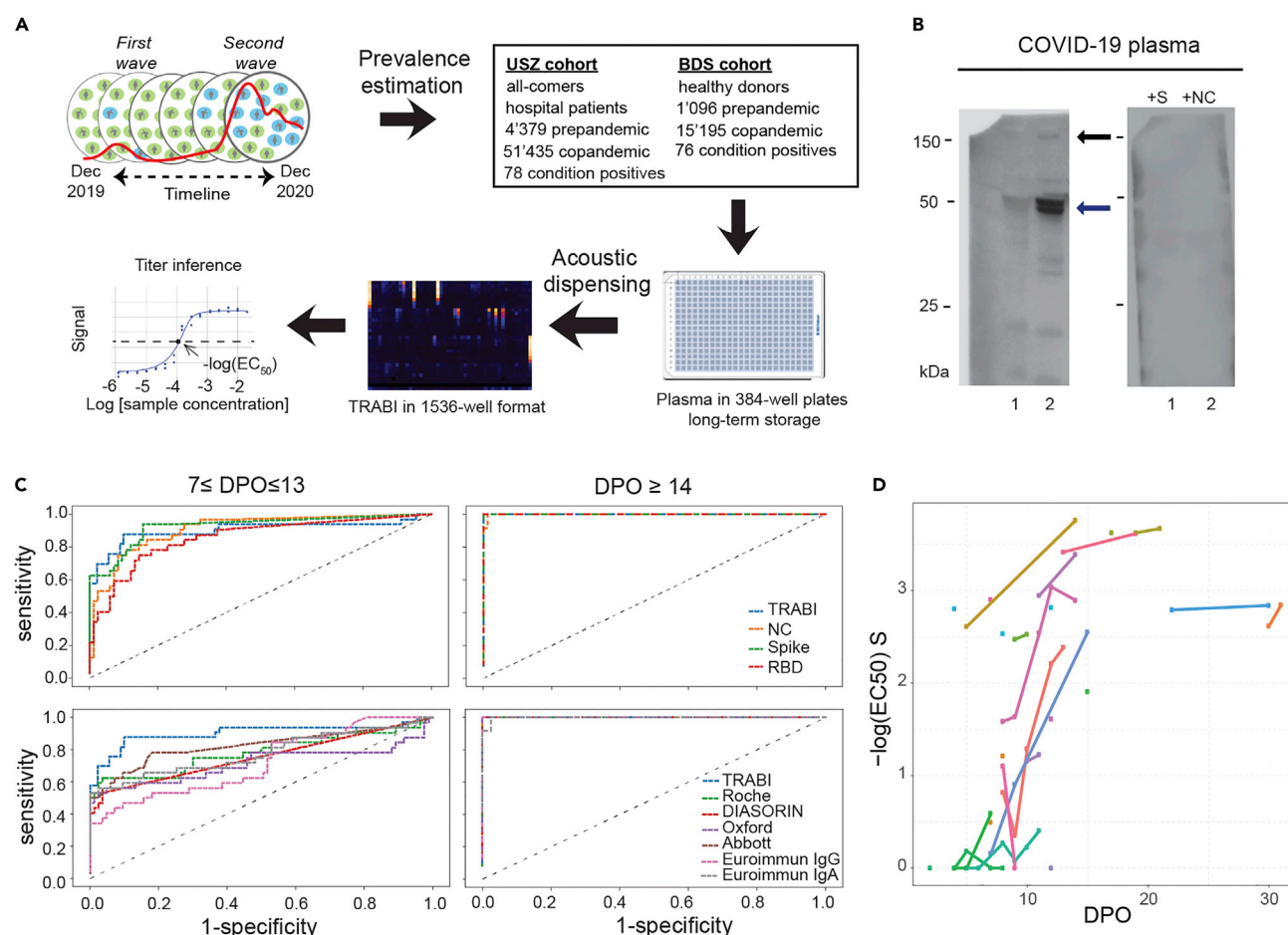


Figure 1. Study overview and establishment of serological pipeline

(A) To estimate the prevalence of CoV2 seropositivity in the population, prepanemic, and copanemic samples from two independent cohorts were analyzed by high-throughput microELISA (TRABI). IgG titers against S, RBD, and NC were determined and the $-\log(\text{EC}_{50})$ was inferred by regression analysis. (B) Vero cells infected with CoV2 (lane 2), but not uninfected cells (lane 1), showed signals corresponding to S (black arrow) and NC (blue arrow, pointing at two bands) when immunoblotted with COVID-19 patient plasma. NC protein undergoes a proteolytic cleavage in SARS-CoV-2-infected VeroE6 cells, resulting in two distinct bands of around 46 and 43 kDa. We confirmed the identity of the two bands by probing with an anti-NC antibody (Sino Biologicals, data not shown). Spiking of COVID-19 patient plasma with recombinant S and NC led to the disappearance of all signals.

(C) Upper panel: Using 53 samples from confirmed patients with CoV2 and 83 prepanemic samples, we assessed the specificity-sensitivity relationship for all antigens individually and after combining all results into a single score (TRABI) using QDA-based posterior probability. Between 7 and 13 dpo, approximately 60% of samples were positive (posterior probability >0.5) at 100% specificity cutoff, whereas 100% sensitivity was reached at ≥ 14 dpo. Lower panel: COVID and prepanemic samples were used to assess the performance of TRABI, commercial tests (Roche, DiaSorin, Abbott, Euroimmun), and an assay developed at the Target Discovery Institute (Oxford). While all tests scored equally at ≥ 14 dpo, TRABI outperformed all other assays at ≤ 13 dpo. (D) Time course of IgG response in 55 samples from 27 patients with COVID-19. IgG antibodies were reliably detectable at ≥ 13 dpo. Colors represent individual patients.

LDA allows us to verify the distributional assumptions more readily (Figures S5C and S5D). Using the distributions of the condition negatives and the condition positives, we computed the posterior probability (i.e. the probability of an individual to being seropositive as modeled via the distribution of the known condition-negatives and known condition-positives) for all data points. The respective ROC curves were then plotted (Figures S5E and S5F). At 100% specificity, we identified 78% of the annotated true positives for the USZ (Figure S5E) and 67% annotated true positives for the BDS cohort (Figure S5F). For both the USZ and the BDS cohorts, the sensitivity increased rapidly with a slight decrease in specificity (at a false positive rate of 0.001, we identified 82% condition positives for USZ and 89% for BDS).

We then applied the QDA-based probability model to estimate the monthly prevalence, from December 2019 to December 2020, using the USZ and the BDS cohorts. No substantial shift above baseline was

Table 1. Characterization of total, copandemic, and prepandemic samples and individuals used in TRABI screening for assay establishment as well as for the seroprevalence estimation using the USZ and the BDS cohorts

		Assay establishment	USZ cohort	BDS cohort	All cohorts
Total	Samples, number	145	55,814	16,291	72,250
	Individuals, number	117	37,745	16,291	54,153
	Mean samples/month (SD)	/	/	/	/
	Median age (IQR), years	/	55 (40–68)	/	/
	Sex, female %	/	47	/	/
	Sex, male %	/	53	/	/
Copandemic	Samples, number	55	51,435	15,195	66,685
	Individuals, number	27	33,366	15,195	48,588
	Mean samples/month (SD)	/	3,957 (1,801)	1,169 (273)	/
	Median age (IQR), years	62 (52–70)	55 (40–68)	42 (28–54)	/
	Sex, female %	37	47	41	/
	Sex, male %	63	53	59	/
Prepandemic	Samples, number	90	4,379	1,096	5,565
	Individuals, number	90	4,379	1,096	5,565
	Mean samples/month (SD)	/	/	/	/
	Median age (IQR), years	/	54 (39–68)	/	/
	Sex, female %	/	48	/	/
	Sex, male %	/	52	/	/

Among the copandemic samples, $n = 78$ samples were annotated as condition positives for USZ and $n = 76$ samples for BDS. The USZ condition-positive samples are part of the seroprevalence estimation while for BDS, the condition-positives are not counted owing to a separate recruitment scheme (see study design for details).

inferred for samples screened until February 2020 (Figure 2C). In March 2020, the USZ-based prevalence increased to 0.5% (95% confidence intervals: 0.3%–0.7%) and to 1.6% (CI95%: 1.2%–2.0%) in April 2020, with blood donors displaying a comparable course of seroconversion, with the prevalence approximating 1.3% in April (CI95%: 1.0%–2.0%). The blood donors then reached a first peak in May 2020, with a prevalence of 1.8% (CI95%: 1.3%–2.5%), while the USZ patients plateaued. Following an initial decline in June (USZ: 1.0% (CI95%: 0.8%–1.2%), BDS: 1.4% (CI95%: 0.6%–2.3%)), the seroprevalence fluctuated at around 0.8% over the course of the summer. These summer months were generally characterized by a low reported incidence (4,106 new PCR-confirmed cases and 16 COVID-19-associated deaths from July 1 to September 30 in the canton of Zurich⁴), until a second wave surged in October. A sharp rise in seroprevalence was observed for November (USZ: 4.0% (CI95%: 3.4%–4.5%), BDS: 2.4% (CI95%: 1.5%–3.2%)) and beginning/mid-December 2020 (USZ: 6.3 (CI95%: 5.5%–7.2%), BDS: 5.1% (CI95%: 4.2%–6.4%)).

To assess the technical reproducibility of TRABI, we repeated the assay on 200 and 112 randomly selected positive and negative samples, respectively. This repeat screen was found to reproduce the original TRABI results ($R^2 = 0.85$, Figures 2D and S6).

Antibodies against the RBD of SARS-CoV can bind to the CoV2 RBD.²⁵ We, therefore, tested whether samples with high anti-CoV2-RBD titers display cross-reactivity with SARS-CoV RBD. For visualization, we binned samples into groups of absent, moderate, and high CoV2 RBD titers ($-\log[EC_{50}] < 1.5$, 1.5–2, and > 2.5 , respectively) and computed their respective QDA-derived posterior probability (same color map as in Figure 2B). For individuals with CoV2 RBD titers < 2 , a small fraction showed binding to SARS-CoV RBD at $-\log(EC_{50}) > 2$ (Figure 2E). However, those with strong binding properties to CoV2 RBD (> 2.5) clustered at high values for SARS-CoV RBD, indicating that some anti-CoV2 RBD antibodies were cross-reactive to SARS-CoV RBD.

Post-stratification for age and sex and removal of patients admitted because of COVID-19

We then stratified the seroprevalence data according to age and sex, for both cohorts (Figure S7A for USZ samples and S7B for BDS samples). As the age and sex distributions of the USZ and BDS cohorts are not

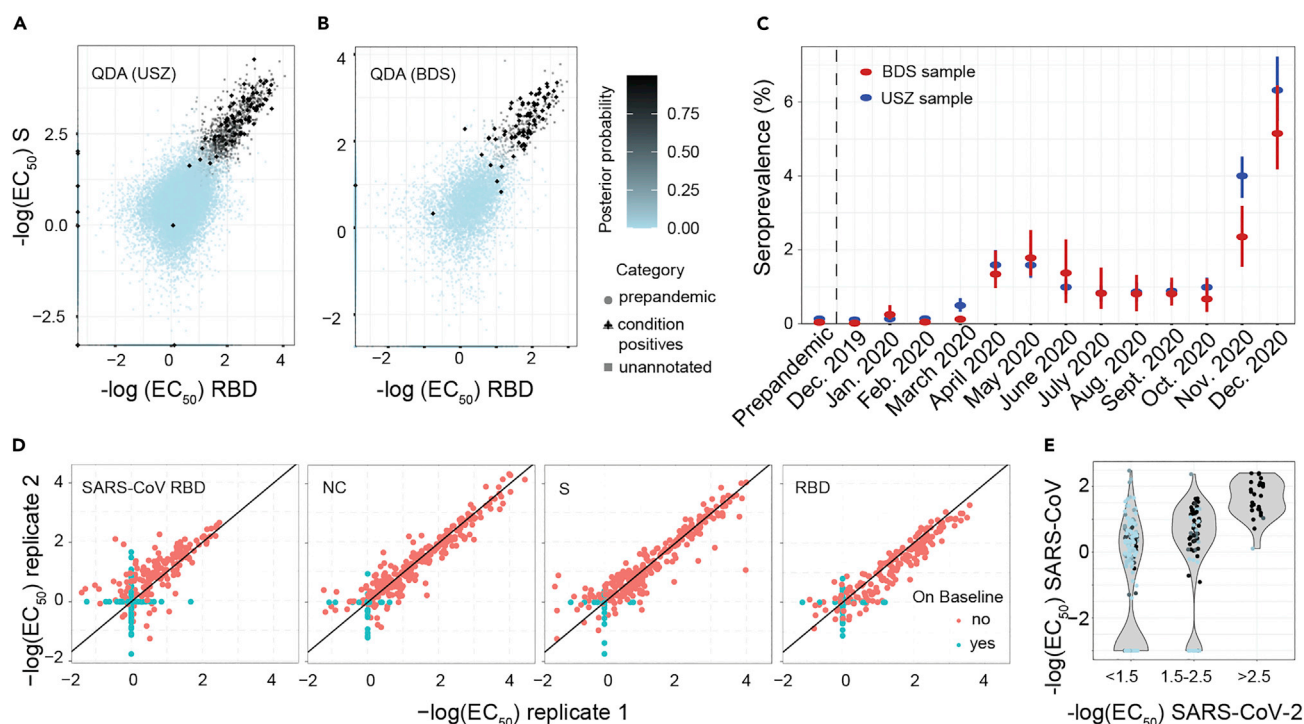


Figure 2. Evolution of CoV2 prevalence in a cohort of Zurich University Hospital (USZ) patients and donors from the blood donation service (BDS)
(A and B) Inflection points of dilution curves, denoted $-\log(\text{EC}_{50})$, of plasma titrated against S and RBD in the USZ and BDS cohorts. Posterior probabilities were calculated using QDA assuming a multivariate Gaussian distribution.
(C) Prevalence of CoV2 seropositivity in prepandemic (before December 2019) and copandemic samples (from December 2019 to December 2020) estimated using the posterior probabilities from the multivariate Gaussian distribution (QDA). Bar: 95% confidence intervals (CI).
(D) TRABI reproducibility was assessed using duplicates run in pairs of independent assay plates.
(E) To assess the potential cross-reactivity of CoV2 seropositive individuals, we tested 200 high-scoring samples and 112 random samples for binding to the RBD of SARS-CoV. CoV2 RBD binders with a high posterior probability (same color maps as in B) segregated within the higher anti-SARS-CoV-RBD titers.

entirely congruent with the distributions within the general population (Figures S3A and 3B), we employed a post-stratification on sex and age using distributional information from the population of the canton of Zurich (Figures 3A and 3B). However, this correction led to only minor changes (maximal effect observed: 5.1% (CI95%: 4.2%-6.4%) unadjusted versus 4.0% (CI95%: 3.1%-5.1%) adjusted for age and sex, for blood donors in December 2020) in the calculated prevalence, suggesting that the two cohorts appropriately reflect the seroprevalence of the adult population.

Additionally, we aimed to assess the extent of a bias posed by patients with severe COVID-19, hospitalized at the USZ for this reason. We thus removed patients (1) admitted to the Infectious Disease and Hospital Hygiene or the Internal Medicine wards or (2) with ICD-10 codes J96.00 ('Acute respiratory failure') and U99.0 ('Special procedures for testing for SARS-CoV-2') from the dataset and re-evaluated the course of seroprevalence for the cohort of hospital patients. We found that patients with COVID-19 contribute to the prevalence observed during both the first as well as the second wave (Figure 3C). Yet, the application of post-stratification on age and sex and the removal of patients with COVID-19 did not change the overall dynamics of seroprevalence.

Antibody waning and cumulative incidence

The decrease in seroprevalence observed after the peak of the first wave is suggestive of waning of antibodies at the population level. The availability of repeated samples from the hospital patients allowed us to explore the titers individually. Using data from 65 individuals with a posterior probability ≥ 0.5 and at least two seroestimates, we observe a decrease in all measurements, except for the S protein, over time, including the compound metric (Figure 3D), in line with a previous report.²⁶ We then estimated the half-life of the decrease of the antibody titer directly from the seroprevalence data, using an extension

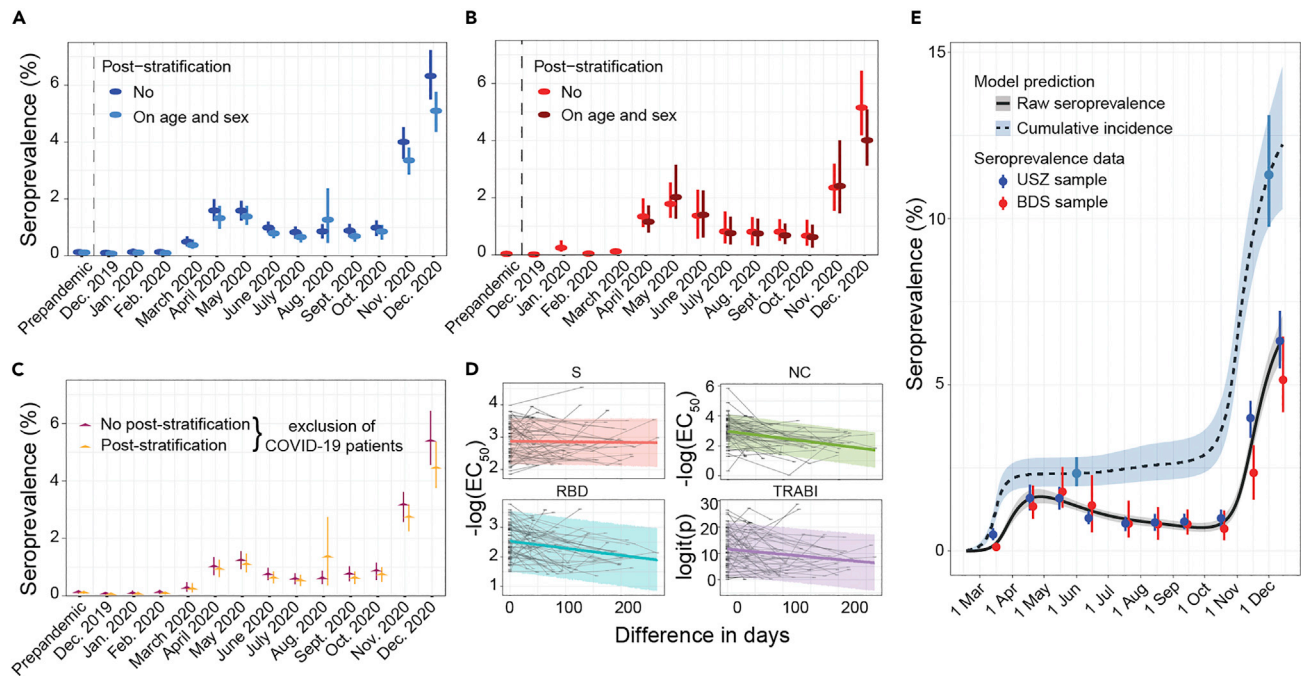


Figure 3. Post-stratification and antibody waning

(A) Seroprevalence in USZ patient cohort after post-stratification on age and sex using the age and sex distributions of the canton of Zurich. Bar: 95% confidence intervals.

(B) Seroprevalence in BDS cohort after post-stratification on age and sex using the age and sex distributions of the canton of Zurich. Bar: 95% confidence intervals.

(C) Seroprevalence in the USZ patient cohort after removal of patients hospitalized because of COVID-19, for both raw seroprevalence and seroprevalence data after post-stratification on age and sex. Bar: 95% confidence intervals.

(D) Antibody waning observed with longitudinal sampling.

(E) Dynamics of SARS-CoV-2 seroprevalence data in USZ and BDS samples between February and December 2020. The seroprevalence is shown in gray (median and 95% CrI). The corresponding model-predicted cumulative incidence, or infection attack rate (IAR), is shown in light blue, with highlighted values on June 1 and December 1.

of the classic Susceptible-Exposed-Infectious-Removed (SEIR) model.²⁷ Assuming an average time to sero-conversion of 14 days,^{28–30} an average generation interval of 5.2 days³¹ and an average time from disease onset to death of 20.2 days,³² the overall half-life observed on the level of the population is 75 (CrI95% 55–103) days (unadjusted) or 88 (CrI95%: 61–128) days (post-stratification for age and sex), similar to what was reported by others.³³ We then computed the cumulative incidence of CoV2, i.e. the seroprevalence corrected for antibody waning, for the population of the canton of Zurich (Figure 3E). The cumulative incidence first raised in March and slowly but gradually increased over the summer period, cumulating to 2.3% (CrI95%: 2.0%–2.8%) in June 2020. A sharp escalation was detectable at the beginning of November, mounding in a cumulative incidence of 12.2% (CrI95%: 10.3%–14.6%) in mid-December 2020. This suggests that over 180'000 people had contracted CoV2 until mid-December 2020 in the canton of Zurich. Thus, the cumulative number of cases detected by PCR (55'375 until 13th of December 2020⁴) is likely to underestimate the true prevalence by approximately factor 3 on average. However, the hidden epidemic ratio (i.e. the number of unobserved cases for each reported case) has changed over time, with a drastic underestimation of cases at the time of the first wave, a clearly improved precision around summer 2020, and a significant underestimation during the second wave (Figure S7C).

Spatiotemporal seromonitoring in University Hospital of Zurich patients covering two waves

We aimed to further depict the evolution of seroprevalence in the canton of Zurich. As we avail of the zip codes, we first mapped the total number of hospital patients per zip code for the months March–July (first wave) and September–December (second wave) 2020 (Figures 4A and 4B), only considering the fraction of patients from the canton of Zurich (Figure S4A). We then investigated the fraction of seropositive hospital patients over the total number of hospital patients per zip code, for the above time periods but restricted

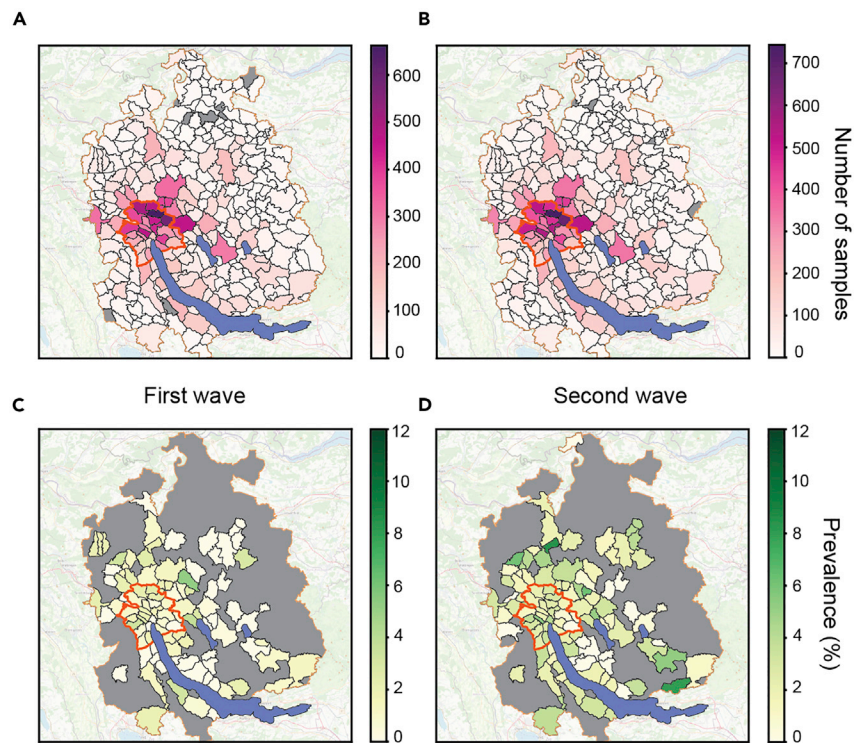


Figure 4. Seroprevalence maps for municipalities in the canton of Zurich

(A) Samples of hospital patients residing in Zurich sorted according to zip codes. Data from January 2020 to June 2020, including the first wave.

(B) Samples of hospital patients residing in Zurich sorted according to zip codes. Data from July 2020 to December 2020, including the second wave.

(C) Seropositive samples of hospital patients residing in Zurich sorted according to zip codes. Data from January 2020 to June 2020, including the first wave.

(D) Seropositive samples of hospital patients residing in Zurich sorted according to zip codes. Data from July 2020 to December 2020, including the second wave. C and D: Only municipalities with at least 50 samples/zip code are displayed. The border of the area of the city of Zurich is surrounded by a dense red line while the municipalities contained within the canton of Zurich, at the border to another canton, are displayed with a lighter orange line.

the analysis to municipalities with at least 50 patients in total, to avoid statistical variability. In line with the overall increased seroprevalence, we observed more than double the number of municipalities (97) showing a prevalence higher than 2% during the second wave, compared to 45 in the first wave (Figures 4C and 4D). This result is indicative of that the epidemic outbreak in Zurich is not focal but extends throughout the canton, with similar rates of increase. The decrease of the fold-change of positive/total cases in the city of Zurich compared to the rest of the canton of Zurich from the first to the second wave (Figure S7D) is substantiating the observation that after a slightly more localized first outbreak and a remission phase, the second wave is characterized by a non-focal spread.

We have additionally analyzed the data by grouping multiple zip codes together, so that we could include all data and did not have to restrict ourselves to at least 50 patients per municipality. While this approach comes with its own set of technical challenges, it allowed us to ensure that we do not miss important information stemming from rural areas with low total patient counts. The results we obtained (see Figure S7E) are consistent with the more rigorous approach detailed above.

Association with demographic and medical data

We then investigated the association between CoV2 seropositivity and disease. First, we retrieved the International Classification of Disease (ICD-10) codes entered by medical encoders of the hospital for insurance purposes, along with age and sex. Using multiple logistic regression in a Bayesian framework, we found positive associations between seropositivity and ICD-10 codes U99.0 ('Special procedures for testing

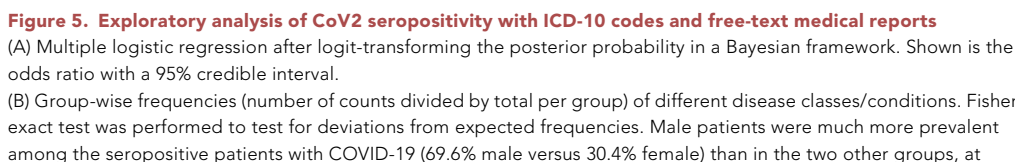


Figure 5. Continued

statistical significance (adjusted p values <0.002). Hypertensive diseases were more prevalent in patients with COVID-19 compared with seronegative patients (adjusted p value = 0.002). p values were adjusted for the number of comparisons conducted (i.e. 45) using post-hoc p value adjustment.⁴³

(C) Flowchart for the inclusion of serologically tested individuals participating in the follow-up online health survey in April/May 2022. A total of 136 individuals provided informed consent and filled the electronic questionnaire, among which 80 reported a known CoV2 infection up to questionnaire completion.

(D) Frequency of symptoms reported by online health survey participants reporting a symptomatic infection prior to April/May 2022 (n = 64).

(E) Date of first infection reported by online health survey participants with a known infection prior to April/May 2022 (n = 80, 2 participants with missing date). Three pandemic waves were reflected in the data: Spring/Summer 2020 (first wildtype CoV2 wave), Fall/Winter 2020/2021 (second wildtype CoV2 wave), and Winter/Spring 2021/2022 (omicron CoV2 wave).

(F) Proportion of online health survey participants reporting to have experienced within the last seven days prior to questionnaire completion, stratified by prior infection status and pandemic wave during which the infection occurred.

(G) Odds ratio of experiencing specific symptoms within the last seven days prior to questionnaire completion in the group of online health survey participants with reported known prior infection compared to the group of participants without known infection, based on multivariable logistic regression models adjusted for age and sex (central estimate: odds ratio, error bars: 95% confidence interval (95%CI)).

(H) Proportion of online health survey participants reporting having received a new medical diagnosis after 2020, stratified by prior infection status and pandemic wave during which the infection occurred.

(I) Proportion of online health survey participants reporting to have experienced within the last seven days prior to questionnaire completion, stratified by symptoms during acute infection.

(J) Proportion of participants reporting having received a new medical diagnosis after 2020, stratified by symptoms during acute infection. Adjusted p values ≤0.01: *. Adjusted p values ≤0.001: **. Adjusted p values ≤0.0001: ***.

for CoV2'), J96.00 ('Acute respiratory failure'), I48.3 ('Typical atrial flutter'), U69.0 ('Pneumonia acquired in the hospital, classified otherwise'), Y82.8 ('Other medical devices associated with adverse incidents'), N17.83 ('Other acute kidney failure'), D64.8 ('Other anemia'), E11.91 ('Type 2 diabetes mellitus without complications'), E87.1 ('Hypo-osmolality and hyponatremia'), and male sex (Figure 5A). However, only U99.0 and J96.00 displayed a consistently distinct positive association after regularization with horseshoe and LASSO priors. Negative associations were found with ICD-10 code Z11 ('Special procedure to the diagnosis of infectious and parasite diseases'), while other codes did not persist after regularization and were probably spurious. Next, to better account for the hierarchically structured web of ICD-10 codes and their interdependencies, we employed a network-based representation,³⁴ aiming to investigate differentially structured nodes in ICD-10 codes, clinical departments, age, and sex, in CoV2-seropositive and seronegative USZ patients. We did not identify any distinctive motif of enriched ICD-10 codes between the seropositive and seronegative patients (Figure S8A), based on topological network scores derived from the Mcode algorithm,³⁵ indicating no greatly altered disease networks as a function of a CoV2 infection. Furthermore, nonlinear Uni-form Manifold Approximation and Projection for Dimension Reduction (UMAP), adjusted for binary data using a cosine metric as well as principal component analysis (PCA) did not reveal any separate cluster for seropositive patients when projecting the variability of the dataset into two-dimensional space, neither when including sex as a feature alongside ICD-10 codes (Figures S8B and S8C) nor upon exclusion of female/male sex (Figures S8D and S8E). The exclusion of patients without ICD-10 codes did not change this, both applying a binary (Figure S8F) as well as an Euclidean distance metric (Figure S8G). Lastly, in a more targeted analysis, we split our dataset into (1) seropositive patients with COVID-19 hospitalized in the Infectious Diseases or Internal Medicine units (n = 240), (2) seropositive patients associated with other clinical wards (n = 483), and (3) randomly selected seronegative patients (n = 631), aiming to interrogate the three groups for differences in potential complications of CoV2 infections recently discussed^{18,36–39} in ICD-10 codes as well as in free-text medical reports. As control indications, we queried for known risk factors (e.g. type II diabetes, obesity, hypertension, COPD, chronic kidney disease) for hospitalization and COVID-19 disease severity^{40–42} and for well-established CoV2 complications (respiratory insufficiency, dyspnea, ARDS, pulmonary embolism, pneumonia).

While the three groups did not display statistically significant differences (Fisher's exact test, p value adjusted for multiple comparisons) in the presence of risk factors, the seropositive patients with COVID-19 (group I) differed significantly from the seropositive patients from other clinical wards (group II, adjusted p value<0.0001) and from the seronegative patients (group III, adjusted p value<0.0001) in known CoV2-associated diseases, illustrated in Figure 5B. None of the neurological or cardiocirculatory conditions investigated showed significant differences between the groups, except for hypertensive diseases that were

Table 2. Population characteristics of serologically tested individuals participating in the online health survey

Individuals, number	136
Median age (IQR), years	55 (41–66)
Sex, female	54 (39.7%)
Sex, male	82 (60.3%)

Indicated are the number of individuals, their median age with interquartile range (IQR), and the number and percentage of individuals of female or male sex.

more prevalent in patients with COVID-19 compared with seronegative patients (adjusted p value = 0.002). Age classes were slightly different in group I compared to group II (p value = 0.0016, Mann-Whitney U test) but not in any other group-wise comparison, with a median age of 58 (IQR: 46–66) years, 53 (IQR: 37–65) years, and 54 (IQR: 39–68) years in the three groups. Male patients were much more prevalent among the seropositive patients with COVID-19 (69.6% male versus 30.4% female) than in the two other groups (Figure 5B; adjusted p value <0.002).

Follow-up online health survey to investigate potential post-COVID-19 condition

Even if patients do not experience overt COVID-19-associated pneumonia or other severe symptoms during acute infection, CoV2-infected individuals may develop post-COVID-19 conditions.^{44–47} We invited hospital patients whose blood had been analyzed at least once by TRABI to participate in a one-time online health survey, conducted from April to May 2022. In 1/354 database entries of hospitalized patients (n = 723 seropositives with TRABI-based probability ≥ 0.5 , n = 631 seronegatives with TRABI-based probability <0.5), e-mail address was available for 666 allowing them to send a survey invitation. Of those, 142 consented to participate and completed the questionnaire, of which 136 contained at least some information that could be used for analysis (participation rate 20.4% of invited, 10.0% of total; see Figure 5C for flowchart and the respective supplementary tables (Tables S3–S5) to document partial missingness of data). These 136 participants, of which 54 (39.7%) were female and 82 (60.3%) were male, had a median age of 55 (IQR: 41–66) years (see Table 2 for population characteristics).

71 individuals (52.2%) had a TRABI-based posterior probability ≥ 0.5 and were considered seropositive, 65 (47.8%) had a posterior <0.5 and were considered seronegative. Within the seronegative population, 98.4% reported no infection prior to blood sampling, while 53.5% of the seropositive individuals reported a known prior infection (Table S3). At the time of blood sampling, the agreement between seropositivity and knowledge of infection was moderate (Cohen's Kappa 0.51, percent agreement 74.8%). Over the full-time frame since the start of the pandemic, 77.6% (52/67) of seropositive individuals and 44.4% (28/65) of seronegative individuals reported an infection up to April/May 2022. To explore the potential effects of CoV2 infection on participants' post-COVID-19 health status, we focused on these 80 individuals reporting an infection, using the 56 individuals without known infection as a comparison.

Amongst those with known CoV2 infection up to April/May 2022, 81.0% reported one or multiple symptoms at the time of infection, while 19.0% reported asymptomatic infection; a result that is consistent with findings by others.^{48,49} Cough, fatigue, and fever were the three most frequent symptoms that were reported during acute infection (Figure 5D). We next assessed the time between the first reported infection and survey completion. The median time since the first infection dated back 525 (IQR: 57–571) days and the time frame included three pandemic peaks (Figure 5E): in Spring/Summer 2020 (first WT CoV2 variant wave), in Fall/Winter 2020/2021 (second WT CoV2 variant wave), and in Winter/Spring 2021/2022 (omicron CoV2 variant wave).

The proportion of hospitalized individuals decreased with time (41.7% in Spring/Summer 2020, 23.5% in Fall/Winter 2020/2021, and 2.9% in Winter/Spring 2021/2022), with diagnosed pneumonia being more frequent in Spring/Summer 2020 (25.0%) than in Fall/Winter 2020/2021 (15.2%) and Winter/Spring 2021/2022 (3.0%, see Table S4).

In terms of recovery, 56.9% of the study participants with known infection by April/May 2022 stated to have fully recovered to their normal health status (45.5% in infected during the first wave in Spring/Summer 2020, 61.3% in infected during Fall/Winter 2020/2021, 56.7% in infected during Spring 2022). Overall, 9.8% reported that they were still experiencing at least some of the initial symptoms at the time of survey completion. 90.2% stated that symptoms lasted up to 3 months, with no study participant experiencing symptoms

lasting between 3 and 6 months. Among those infected with WT CoV2, 11.4% reported that they were still experiencing symptoms more than 12 months after infection. The proportion with ongoing symptoms was comparable between infection waves, albeit slightly lower for the omicron wave (10.0% in Spring/Summer 2020, 13.0% in Fall/Winter 2020/2021, and 7.1% in Winter/Spring 2021/2022). Three individuals (8.3% of those with known infection during the first two waves) were reported to have been diagnosed with post-COVID-19 condition (long COVID).

The prevalence of symptoms within the past seven days (before completing the survey) among the previously infected group was highest for fatigue, sleeping problems, reduced performance, cough, and concentration (Figure 5F). Meanwhile, when comparing symptom prevalence among previously infected with those that had never experienced an infection, cough, gastrointestinal symptoms, skin problems, nervousness, myalgia, arthralgia, and depression were reported more frequently by participants, among others (Figure 5G, logistic regression, adjusted for age and sex). However, these differences did not reach statistical significance, with the exception of cough (odds ratio = 10.7, p value = 0.026, adjusted for age and sex). A higher number of participants would likely clarify some of the trends observed here.

We next asked the patients to report on new medical diagnoses that they have obtained after 2020. Here, we aimed to find out whether the prevalence of disease classes was fundamentally different in patients after infection with CoV2, while using the non-infected group as control. The most commonly medically diagnosed conditions of those with infection were related to skin, lung, thyroid, kidney, and immune system (Figure 5H), while none of the comparisons with the non-infected group reached statistical significance (logistic regression, adjusted for age and sex). Of note, those who got infected during the first wave displayed a particularly high frequency of neurological diagnoses, and a comparatively low proportion of participants with new medical diagnoses was observed in those infected during the Winter/Spring 2021/2022 wave.

Then, we assessed the participants' health status using the EuroQol 5-dimension 5-level instrument (EQ-5D-5L) and the EuroQol visual analogue scale (EQ-VAS), where increased EQ-5D-5L and EQ-VAS scores correspond to increased/better health. Overall, there was no statistically significant difference in EQ-5D-5L and EQ-VAS scores between individuals reporting a known infection (mean EQ-5D-5L: 0.87, SD: 0.19; mean EQ-VAS: 75.00, SD: 15.83) than those not infected (mean EQ-5D-5L: 0.81, SD: 0.17, p value = 0.13; mean EQ-VAS: 70.30, SD: 20.88, p value = 0.15; logistic regression, adjusted for age and sex; see Table S5).

Lastly, we repeated these analyses to compare the longer-term health impacts between individuals with symptoms during acute infection ($n = 64$) and individuals with asymptomatic infection ($n = 30$). Both symptoms experienced during the last seven days (Figure 5I) as well as new medical diagnoses (Figure 5J) did not display statistically significant differences between the two groups. Similarly, EQ-5D-5L and EQ-VAS scores between symptomatic (mean EQ-5D-5L: 0.87, SD: 0.19; mean EQ-VAS: 77.54, SD: 11.73) and asymptomatic individuals (mean EQ-5D-5L: 0.86, SD: 0.17; mean EQ-VAS: 69.00, SD: 21.41) did not differ significantly (p value = 0.879 for EQ-5D-5L and p value = 0.02 for EQ-VAS; logistic regression, adjusted for age and sex). Due to the limited sample size, the findings regarding symptoms, new medical diagnoses, and longer-term health impairment need to be interpreted with caution. We found no evidence for a difference in longer-term health outcomes between individuals with symptomatic and asymptomatic acute infection. These results suggest that post-COVID-19 condition, with symptoms lasting longer than twelve months, occurs in approximately 10%.

Prevalence of anti-CoV2 antibodies in prepandemic samples

5'475 prepandemic plasma samples (4'379 USZ patients and 1'096 healthy blood donors) were examined for the presence of cross-reactive antibodies against S, RBD, and NC of CoV2. Several individuals had a strong antibody response against a single antigen and an absence of binding to other antigens, reflected in a low posterior probability but high $-\log(\text{EC}_{50})$ value. We then directly compared prepandemic and copandemic samples in the USZ cohort on the basis of single antigens and their respective posterior probabilities. When focusing on samples with high values for single assays, we observed an enrichment of high posterior probabilities in the pandemic but not in the prepandemic group (Figure 6A). Among samples with individual $-\log(\text{EC}_{50})$ values above 2 in May and June 2020, 76% (S), 80% (RBD), and 22% (NC) had a posterior probability >0.5 . In the prepandemic samples, maximally 1 sample with an individual assay level

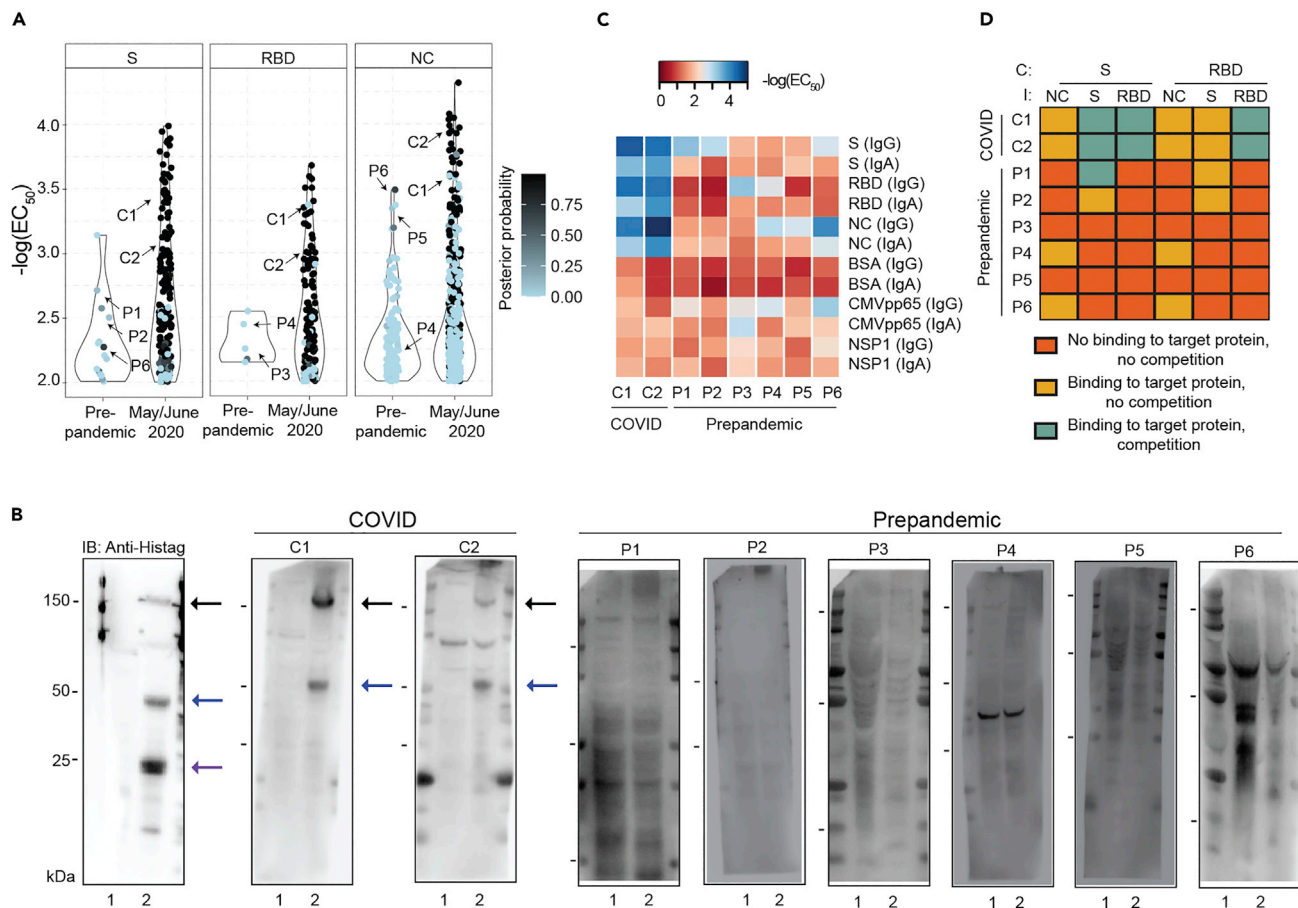


Figure 6. Characterization of prepanemic samples

(A) Posterior probability was calculated assuming a Gaussian distribution and visualized for individual antigens (S, RBD and NC) for prepanemic samples vs. copandemic USZ samples drawn in May and June 2020. Prepanemic samples exhibited a low posterior probability as they typically reacted against single antigens, leading to low rankings in a composite metric. For further testing, comparative samples were chosen from the prepanemic era and from May and June 2020. Arrows point to samples of individuals used in (B), (C), (D). P1-6: prepanemic 1-6; C1-2: COVID1-2.

(B) Western Blot analysis of two samples from May/June 2020 ("COVID 1" or C1 and "COVID 2" or C2) and several prepanemic samples (P1-6). Anti-his-tag antibody was included as a positive control. Lane 1 = non-transfected Expi293F cell lysate; Lane 2 = Expi293F cell lysates expressing his-tagged S, NC, and RBD proteins. Black arrows: S; blue arrows: NC; purple arrow: RBD. The molecular weights (in kDa) are depicted on the left side and refer to the bands shown in all blots.

(C) ELISA assays on the same samples as in B, using CoV2 S, NC, RBD, and NSP1 as well as control proteins (BSA, CMV pp65), shown in the form of a heatmap where the $-\log(EC_{50})$ of the sample dilution is depicted.

(D) Competition assays were carried out in the same samples as in B and C. Competition (C) was performed with S (0.04-88 nM) or RBD (0.7-1,350 nM) and plates were immobilized (I) with S, RBD, or NC. Data from duplicates is depicted using the following qualitative categories: No binding to target protein, no competition (orange). Binding to target protein, no competition (yellow). Binding to target protein, competition (turquoise). Soluble antigens suppressed the ELISA signal in the COVID samples but not in the prepanemic sample (except for P1 where soluble S competed with the immobilized S), showing that the antibodies present in the latter had lower affinities for CoV2 targets.

above 2 had a posterior probability above 0.5. This enrichment is suggestive of a substantial performance improvement when using the combined metric in the USZ cohort.

We then compared the immunochemical properties of six prepanemic samples with high binding to S, RBD, or NC to two samples of confirmed COVID-19 (COVID 1 and 2, see annotation in Figure 6A). The COVID-19 samples, but not the prepanemic samples, recognized in Western blots the S and NC antigens of CoV2 expressed by Expi293F cells maintained as suspension culture (Figure 6B). Additional ELISAs performed on the same samples confirmed the initial findings (Figure 6C) including intact binding to the RBD. The discrepancy between ELISA and Western Blot suggests that the RBD is a highly conformational epitope lost upon boiling and SDS denaturation.

To further probe the specificity of the findings, we also carried out competitive ELISAs on prepandemic and patients with COVID-19. First, we determined plasma concentrations close to the EC_{50} . Then we pre-incubated appropriately diluted samples with various concentrations of S and RBD (0.04–88 and 0.7–1,350 nM, respectively). Samples were then transferred onto ELISA plates coated with S, RBD, and NC. The concentration-dependent displacement of the measured optical density was then interpreted and categorized into three distinct classes: (1) No binding to the target protein, no competition. (2) Binding to the target protein, no competition. (3) Binding to the target protein, competition (Figure 6D). We found that both soluble S and the RBD caused a concentration-dependent depletion of the RBD in COVID samples. The S signal could not be depleted with RBD, indicating the presence of epitopes other than the RBD. One prepandemic sample (#1) displayed competition of the S signal with soluble S but not with soluble RBD. Other prepandemic samples did not show competition at all, suggesting that their reactivity was due to high concentrations of low-affinity antibodies cross-reacting with CoV2 S.

Identification of seropositives in healthy donors and clonality of anti-S immune response

TRABI enabled the identification of 189 CoV2 seropositive blood donors that underwent regular blood donation at the blood donation service of Zurich (Figures 2B and 2C) despite clear serological indications of past infection and antibody titers in the same range as those of PCR-confirmed convalescent individuals (Figure 7A). We assessed IgG and IgA antibodies to S, RBD, and NC as well as responses to multiple control antigens, in 4 healthy blood donors and 4 convalescent individuals recruited to the BDS. We observed the binding of IgG antibodies in blood donors and convalescent individuals against S, RBD, and NC, with usually lower IgA titers. No binding against the CoV2 non-structural-protein 1 (NSP1), or against BSA was observed.

To further validate the seropositivity in healthy blood donors, we employed an orthogonal methodology that allows antibody/antigen interactions to be probed in solution, without any immobilization of antigens to a surface.¹⁹ Samples of CoV2 convalescent individuals, healthy donors, and controls were pre-incubated with fluorescently conjugated RBD protein. We then monitored the increase in the effective molecular weight of an Alexa 647-labeled RBD construct in solution upon complex formation with an antibody present in the patient sample. This was achieved by measuring the associated decrease in its molecular diffusion coefficient upon binding using a microfluidic platform. While no change in diffusion coefficient or the associated hydrodynamic radius was observed in control samples, all ELISA-positive samples from convalescent and healthy donors indicated a clear binding of antibodies to RBD (Figure 7B). We confirmed these findings by using the samples of several healthy blood donors and convalescent individuals as primary antibodies in Western Blot and detected bands for both S and the NC in the Expi293 cells overexpressing the viral proteins but not in the Expi293 control lysate (Figure 7C).

To obtain a rough estimate of the clonality and epitope specificity of the immune response raised against the S protein, we conducted an ELISA-based soluble antigen competition. Competition with the RBD leads to a decrease in ELISA signal for RBD but not for S or NC in both convalescent individuals and healthy blood donors (Figure 7D). Conversely, competition with S decreased the signal for both S and the RBD, suggesting the presence of antibodies targeting multiple S epitopes, including RBD. Therefore, the immune response against S was polyclonal and involved multiple viral epitopes.

DISCUSSION

Using a high-throughput CoV2 serology pipeline, we draw a detailed picture of the evolution of CoV2 seroprevalence in a large central-European metropolitan area. If antibody titers were stable after infection, the seroprevalence would reflect the entirety of the population infected since the inception of the pandemic. However, anti-CoV2 titers were found to decay in multiple studies,^{12–16,33} with a half-life of approximately 106 (CI95% 89 to 132) days,¹² 76 to 156 days,³³ and others suggesting an even shorter half-life of 26–60 days.¹⁴ This decrease in titers over time was confirmed in neutralization assays, shown in various studies.^{13,15,16} Indeed, between April and July 2020 the prevalence of seropositivity fell by $\approx 60\%$ in our cohorts, which confirms the waning of humoral immunity at the population level. Using an extended SEIR model, we estimated that the population-wide half-life of seropositivity is 75 (CI95% 55–103) days (unadjusted seroprevalence data) or 88 (CI95%: 61–128) days (after post-stratification for age and sex).

If our sampling methodology suffers from systematic errors, the cohorts sampled here may not be representative of the population studied. In order to minimize such issues, we surveyed two non-overlapping

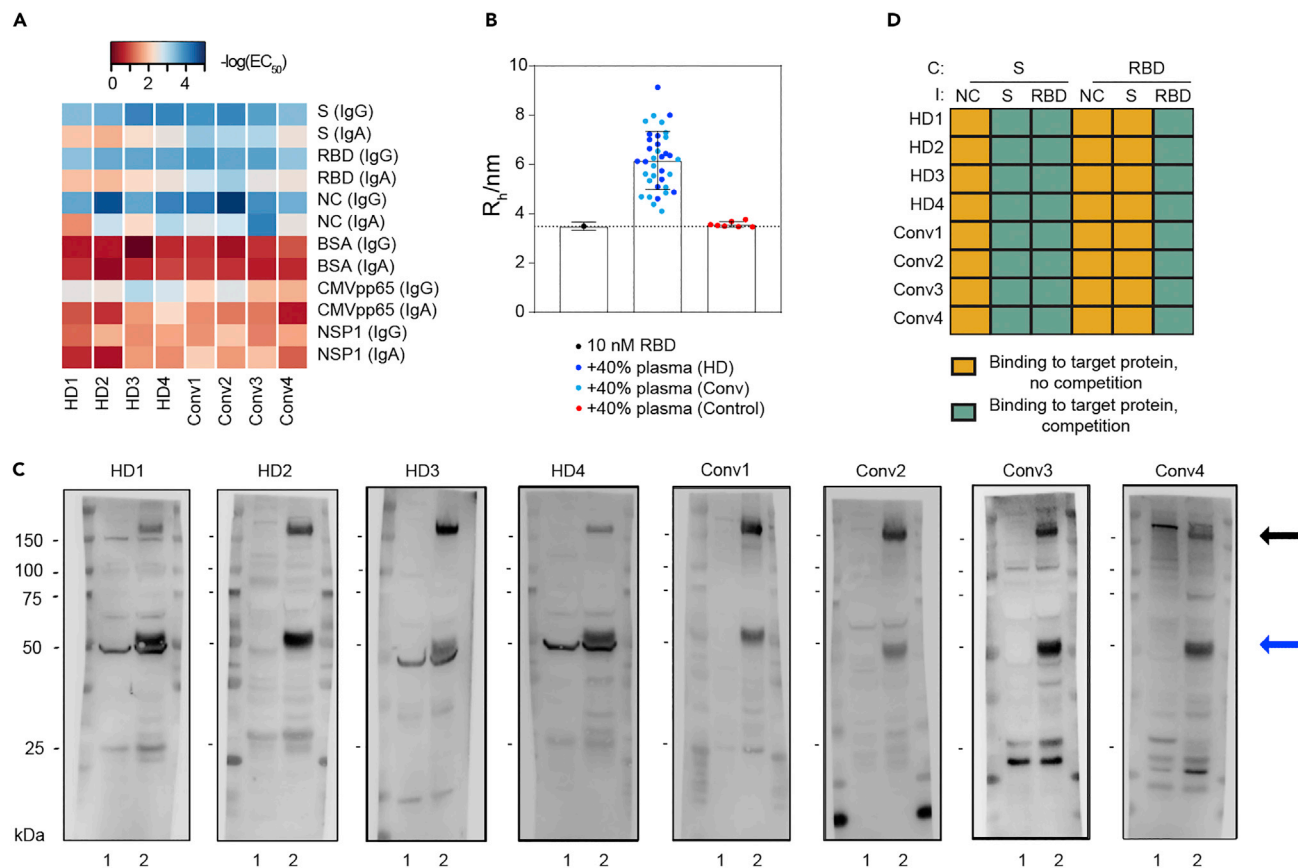


Figure 7. Assay validation in solution and clonality of anti-S immune response

(A) ELISA assays of healthy blood donors vs. convalescent individuals depicted as heatmap. The $-\log(\text{EC}_{50})$ depicts the sample dilution at which half-maximum binding occurs. S, RBD, and NC are strongly bound by both healthy donors (HDs) as well as convalescent (Conv) individuals.

(B) Microfluidic-based assessment of binding between an Alexa 647-labelled RBD antigen and antibodies in solution. No change in diffusion coefficient or the associated hydrodynamic radius was observed in control samples, while all ELISA-positive samples from convalescent and healthy donors indicated a clear binding of antibodies to RBD, confirming the ELISA-based results. Shown are mean \pm SE.

(C) Western Blot analysis of the same individuals tested in (A). Lane 1 = non-transfected Expi293F cell lysate; Lane 2 = Expi293F cell lysates expressing his-tagged S, NC, and RBD proteins. Black arrows: S. Blue arrows: NC. The molecular weights (in kDa) are depicted on the left side and refer to the bands shown in all blots.

(D) Competitive ELISA using RBD or S for soluble competition with antibodies in plasma from the same individuals as in (A) and (C). Data is depicted using the following qualitative categories: Binding to target protein, no competition (yellow). Binding to target protein, competition (turquoise). Competition (C) with S or RBD did not change the signal upon immobilization (I) with NC, while competition with S resulted in a decrease in signal upon immobilization with S as well as with RBD. Conversely, competition with RBD only competed signal when immobilized with RBD, not with S, indicating the presence of antibodies against S domains other than RBD.

cohorts: hospital in- and outpatients and healthy blood donors. Neither cohort can be assumed to represent a representative random sample of the population. However, post-stratification by age and sex led to only minor changes in seroestimates, indicating that our cohorts are largely representative of the adult population of the canton of Zurich. However, we have not investigated the extent of CoV2 spread in children in the canton of Zurich, which was recently done by others.⁵⁰

The dynamics of the seroepidemiology confirm that the outbreak followed three distinct phases. The cumulative incidence rose during the first wave in spring 2020, with 2.3% (CrI95%: 2.0%-2.8%) having contracted CoV2 by June 2020. There was a modest increase over the summer months, followed by a rapid rise in late 2020. We estimate that 10.3-14.6% had undergone an infection with CoV2 by mid-December 2020.

Thereby, we could delineate the precise serological status in the population of the canton of Zurich in a continuous manner, rather than on single points in time. These estimates of CoV2 antibodies were

performed on a highly sensitive immunoassay (TRABI) that combines antibody measurements against three CoV2 proteins in a QDA-based compound metric, a system developed in house. In view of the critique leveled at past serological studies,^{51,52} we have gone to great lengths to assess and validate our technology, using several orthogonal techniques. A recent publication⁵³ has shown pre-existing anti-CoV2 antibodies in unexposed humans. Antibody sizing^{19,54} and immunoblots, however, point to fundamental differences between prepandemic seropositivity and the immune responses of CoV2-infected individuals. While the latter consistently showed high-affinity responses that were clearly visible in Western blotting, the few seropositive prepandemic sera were unanimously negative in Western blotting, and equilibrium displacement ELISA of one prepandemic plasma sample suggested a much lower affinity despite similar antibody EC₅₀ titers. We conclude that any immune response in uninfected individuals, whether it represents cross-reactivity with common-cold coronaviruses or something else, is of inferior quality and may less likely to be protective. A blinded comparison with commercial test kits showed that our approach was suitable for large-scale epidemiologic studies and that the compound metrics did indeed lead to a power gain, as shown by the enrichment of samples with high posterior probabilities in excess of the single assays during the epidemic.

The comparably low seroprevalence of CoV2 in the canton of Zurich, in particular during the first wave, is compatible with other more affected regions, based on the reported IFR, in Switzerland⁵⁵ and in European areas with similar medical infrastructure.⁵⁶ While some large-scale serological surveys performed throughout the globe revealed CoV2 spread slightly exceeding the values we observed in Zurich,^{7,11,57} other studies identified regions with seroprevalence surpassing 50%, e.g. in some areas in the Amazonas state in Brazil¹² or in slums in Mumbai, India.⁵⁸ Yet, since antibody waning has been reported in multiple instances,^{11–16,33} discrete seroestimates may reflect snapshots of the immunity status of a population at a certain time, rather than the true cumulative case incidence. Conversely, we have accounted for antibody waning, using a model fit developed by data obtained through continuous CoV2 seromonitoring. Thereby, we were able to derive the cumulative incidence rate for both the first and the second wave of the epidemic in the canton of Zurich and have shown that the nation-wide antigen testing underestimates the true number of CoV2 infections by approximately factor 3, similar to what was found in France.⁵⁹

By now, vaccination campaigns in the canton of Zurich, throughout Switzerland, and in multiple places across the globe have rapidly advanced, reaching a stage where novel booster candidates (e.g. Moderna mRNA-1273.211 and Pfizer COVID-19 Vaccine, Bivalent (Original and Omicron BA.4/BA.5), i.e. bivalent booster vaccines), with expected superior activity against many known variants of concern, have become available. Yet, the continuous monitoring of the antibody response will remain a crucial component to epidemiologically assess the extent of immunity within our population over time,^{60,61} in children as well as in adults. Our TRABI assay may be particularly meaningful since we can distinguish between natural infections (eliciting an antibody response also against the NC protein) and vaccination-induced immunity (targeting the S protein). Our cohort of hospital patients will be further surveyed for the surge of unexpected clinically relevant sequelae that may be associated with an infection of CoV2. Initial analyses performed on our dataset did not reveal clusters of disease entities associated with CoV2 infection, compared with patients with no history of CoV2 seropositivity. Along these lines, our data do not indicate an increased prevalence of Parkinson's disease upon CoV2 infection, an association suggested by recent case reports.^{62–64} Interestingly, male patients were overrepresented in the cohort with severe disease requiring hospitalization although infections seem to be roughly equally distributed between female and male. As a clear limitation of our approaches, maladies that do not require treatment at a university hospital center may be altogether missed since the patients may be referred to a practitioner outside the university setting, whereby the occurrence of disease would not be entered into the hospital database system. Moreover, pseudonymized, i.e. linked-anonymized and de-identified, records of patient data, used for the protection of sensitive information from patients, do not allow to gain access to detailed non-parameterized files, such as e.g. full-text reports including sensitive patient identity-related information, and the presence of a diagnosis may be missed.

Meanwhile, we were able to provide additional depth regarding the post-COVID-19 health status of patients whom we had identified as seropositive using the TRABI assay or who self-reported an infection with CoV2 up to April/May 2022 through a standardized online health survey. We found that 11.4% of those reporting an infection in the first two pandemic waves (Spring/Summer 2020 and Fall/Winter 2020/2021) still complained about ongoing symptoms after >12 months after infection, and 8.3% had received a

diagnosis of post-COVID-19 condition ('long COVID'). While numbers in the literature cover a wide range of about 14-75% potentially affected by post-COVID-19 condition up to one year after diagnosis,^{47,65-69} our findings are comparable to those of other population-based studies.^{47,70} Online health survey participants with known infection reported several symptoms and new medical diagnoses more frequently than those without infection, but differences were not statistically significant and no differences in health status (EQ-5D-5L and EQ-VAS) were observed between these groups. Similarly, no significant differences in long-term outcomes between individuals with symptomatic and asymptomatic infection were identified, suggesting that the occurrence of post-COVID-19 may be independent of symptoms during acute infection. Yet, these analyses are limited by the participation rate resulting in a relatively small sample size. Certain consequences of CoV2 infection—potentially CoV2 clade dependent²¹—may take more time to manifest and large numbers of patients may need to be assessed to perform solid statistical analyses due to the heterogeneous clinical picture^{18,71-73} and the phenotypic heterogeneity of post-acute COVID-19 sequelae.⁷⁴ Furthermore, it cannot be excluded that selection effects or potential residual confounding may have influenced the findings of the survey. However, our key findings—emerging from comparisons with a much needed control group ('never infected') often omitted in observational studies⁷⁵—are consistent with the literature and underpin that longer-term symptoms and complications post COVID-19 are an important concern for patient care and public health.

Ultimately, as much of a catastrophe as CoV2 has been, we are not immune to future epidemic outbreaks of other viral diseases potentially far worse. Yet, a multidimensional, comprehensive, i.e. evidence-based understanding of a public health threat, such as CoV2, to which this study contributes, may provide crucial epidemiological tools to prevent an epidemic at an early stage, to save lives and increase life quality throughout the world.

Limitations

The enrollment of participants in a prospective observational cohort study, thought to be representative of the entire population, presents a set of challenges.^{76,77} While avoiding the conventional enrollment bias⁷⁸ (which may have been particularly important in 2020), we made use of surplus samples collected for routine diagnostics ('cross-departmental university hospital patient cohort') and blood donations ('cohort of healthy blood donors'). Limitations inherent to our pragmatic study design⁷⁹ relying on 'further use' of bio-specimens were addressed where appropriate, e.g. by adjusting the age and sex distribution of the study collective to the adult population of the canton of Zurich. The congruency between hospital patients and blood donors has boosted our confidence that these results provide an accurate picture of the cumulative incidence in the population of the canton of Zurich in the time frame reported. The conclusions drawn from the follow-up health survey conducted in April/May 2022 are limited most importantly by the sample size. However, the observation that post-COVID-19 condition, with symptoms lasting longer than twelve months, occurs in approximately 10%, is consistent with recent reports employing alternative enrollment schemes.^{47,70}

STAR★METHODS

Detailed methods are provided in the online version of this paper and include the following:

- KEY RESOURCES TABLE
- RESOURCE AVAILABILITY
 - Lead contact
 - Materials availability
 - Data and code availability
- EXPERIMENTAL MODEL AND SUBJECT DETAILS
 - Ethics statement
 - Study design and sampling
 - Sample annotation and identification of condition positives
- METHOD DETAILS
 - High-throughput serological screening
 - Counter screening using commercial and custom-designed platforms
 - Protein production
 - Assay validation
- QUANTIFICATION AND STATISTICAL ANALYSIS

- Analysis of data derived from high-throughput serological screen
- Epidemiological modelling
- Online health survey

SUPPLEMENTAL INFORMATION

Supplemental information can be found online at <https://doi.org/10.1016/j.isci.2023.105928>.

ACKNOWLEDGMENTS

Institutional core funding by the University of Zurich and the University Hospital Zurich (Switzerland), Swiss National Science Foundation (SNF) grant #179040 as well as Driver Grant 2017DRI17 of the Swiss Personalized Health Network to AA; funding by a grant of the NOMIS Foundation, the Schwyzer Winiker Stiftung, and the Baugarten Stiftung (coordinated by the USZ Foundation, USZF27101) to AA and ME. The robotic rig was acquired with a R'Equip grant from the Swiss National Science Foundation to AA. Screening methodologies had been developed thanks to the support of an Advanced Grant from the European Research Council to AA. Funding by grants of Innovation Fund (INNOV00096) of the University Hospital Zurich, Switzerland, to AA, AvE, DS, EPM, ME, and OB. Utilization of the Fluidity One-W was kindly granted by Fluidic Analytics, Cambridge, UK. This work was supported by ETH Research Grant ETH-23 18-2 and a Ph.D. fellowship by Boehringer Ingelheim Fonds to KS. RPBJ acknowledges funding by the EPSRC for Doctoral Training in Sensor Technologies and Applications (grant EP/L015889/1). ICM acknowledges funding by the Swiss Government FCS. CC was funded by a Swiss Academy of Medical Sciences fellowship (#323530-191220). GFXS was supported by COVID-19 Emergency Fund of the Director of PSI. TM is supported by Cancer Research UK grants C20724/A14414 and C20724/A26752 to CS (Oxford). Oxford work was supported by the MRC and Chinese Academy of Medical Sciences Innovation Fund for Medical Science, China Grant 2018-I2M-2-002. GRS is supported as a Wellcome Trust Senior Investigator (grant 095541/A/11/Z) and receives funding from the National Institute for Health Research Biomedical Research Centre Funding Scheme. CA received funding from the European Union's Horizon 2020 Research and Innovation Programme - project EpiPose (No 101003688) and the Swiss National Science Foundation (grant 196046). TB received funding from the European Union Horizon 2020 research and innovation program under the Marie Skłodowska-Curie grant agreement No 801076, through the SSPH+ Global PhD Fellowship Program in Public Health Sciences (GlobalP3HS) of the SSPH+. All authors wish to thank their entire teams for their support in the lab. Linda Irpinio, André Wethmar, and Andra Chincisan are acknowledged for help in the lab and with data processing. We are grateful to Elisabeth J. Rushing (USZ) for proofreading the article, to Guido Bucklar, Michael Fetzter, Katie Kalt, Karin Edler, Roland Naef, and especially Patrick Hirschi (USZ) for their help with hospital data, and to Didier Trono for helpful insights and discussions. Michael Weisskopf, Antje Thiem, Regina Grossmann, and the team of the Clinical Trials Center (CTC) of the USZ are acknowledged for their help with sample acquisition and protocols. Above all, we are grateful to all blood donors and hospital patients for helping us conduct this study. Lastly, Vishalini Emmenegger (ETH Zurich) offered insights, advice and kind help with illustrations, and supported, accompanied, and inspired the work with love.

AUTHOR CONTRIBUTIONS

Collected and processed the biological specimens, prepared and carried out the high-throughput screenings, maintained the machines: ME, DS, BD, JG, AW, MI, JD, LB, LM, and CZ. Analyzed data from the high-throughput serology: DL, RJ, IX, ME, AA. Carried out follow-up ELISAs and competitive ELISAs: EDC, RM, ME. Carried out Western Blots: EDC, CT, AGG. Carried out and interpreted experiments in solution using microfluidics diffusional sizing technology: MMS, ICM, CKX, GM, TJPK, VK, ME, AA. Collected samples from COVID-19 patients for the establishment of serology: ILD and DJS. Coordinated the sample acquisition and processing from the Institute of Clinical Chemistry: AvE and LS. Coordinated the sample acquisition and processing from the blood donation services: BF and JG. Coordinated and performed high-throughput ELISAs for comparison in Oxford: DE, StH, DIS. Coordinated and performed CoV2 serological assays using commercial platforms: LS, KS, AvE, EPM, and OB. Produced proteins: DIS, NBB, RO, TM, FP, DH, KL, EDC, JDH, FL, AMR, SH, GS. Carried out the epidemiological modeling: CA, JR, ME. Designed, conducted, analyzed, and interpreted the online health questionnaire: TB, DM, MAP, ME. Coordinated the correspondence with the ethics committee of the Kanton of Zurich: RR, JN, ME. Produced and redacted the figures: AA, RJ, DL, EDC, ME. Conceived the idea of creating a biobank of plasma samples, supervised the study on a daily basis, proposed primary and

confirmatory experiments, advised on best lab practices, on control experiments, and on data interpretation: AA. Wrote abstract, introduction, and discussion: AA. Wrote a first draft of the Results part of the article: ME. Advised on and corrected the [results](#) section: AA. All authors contributed by reviewing the first draft, approved the final version, and consented to be accountable for the work.

DECLARATION OF INTERESTS

TPJK is a member of the board of directors of Fluidic Analytics. AA is a member of the board of directors of Mabyon AG which has funded antibody-related work in the Aguzzi lab in the past. All other authors declare no competing interests.

Received: August 16, 2022

Revised: December 18, 2022

Accepted: January 3, 2023

Published: February 17, 2023

REFERENCES

- Lamparter, D., Jacquat, R.P.B., Riou, J., Menges, D., Ballouz, T., and Emmenegger, M. (2022). Code repository for SARS-CoV-2 seroprevalence study. 10.5281/ZENODO.7454292.
- Zhou, P., Yang, X.L., Wang, X.G., Hu, B., Zhang, L., Zhang, W., Si, H.R., Zhu, Y., Li, B., Huang, C.L., et al. (2020). A pneumonia outbreak associated with a new coronavirus of probable bat origin. *Nature* 579, 270–273. <https://doi.org/10.1038/s41586-020-2012-7>.
- Zhu, N., Zhang, D., Wang, W., Li, X., Yang, B., Song, J., Zhao, X., Huang, B., Shi, W., Lu, R., et al. (2020). A novel coronavirus from patients with pneumonia in China, 2019. *N. Engl. J. Med.* 382, 727–733. <https://doi.org/10.1056/nejmoa2001017>.
- Statistisches Amt Kanton Zuerich (2020). Open ZH github. https://github.com/openZH/covid_19.
- Kucirka, L.M., Lauer, S.A., Laeyendecker, O., Boon, D., and Lessler, J. (2020). Variation in false-negative rate of reverse transcriptase polymerase chain reaction-based SARS-CoV-2 tests by time since exposure. *Ann. Intern. Med.* 173, 262–267. <https://doi.org/10.7326/M20-1495>.
- He, X., Lau, E.H.Y., Wu, P., Deng, X., Wang, J., Hao, X., Lau, Y.C., Wong, J.Y., Guan, Y., Tan, X., et al. (2020). Temporal dynamics in viral shedding and transmissibility of COVID-19. *Nat. Med.* 26, 672–675. <https://doi.org/10.1038/s41591-020-0869-5>.
- Pollán, M., Pérez-Gómez, B., Pastor-Barriuso, R., Oteo, J., Hernán, M.A., Pérez-Olmeda, M., Sanmartín, J.L., Fernández-García, A., Cruz, I., Fernández de Larrea, N., et al. (2020). Prevalence of SARS-CoV-2 in Spain (ENE-COVID): a nationwide, population-based seroepidemiological study. *Lancet* 396, 535–544. [https://doi.org/10.1016/S0140-6736\(20\)31483-5](https://doi.org/10.1016/S0140-6736(20)31483-5).
- Carrat, F., De Lamballerie, X., Rahib, D., Blanché, H., Lapidus, N., Artaud, F., Kab, S., Renuy, A., Szabo De Edelenyi, F., Meyer, L., et al. (2020). Seroprevalence of SARS-CoV-2 among adults in three regions of France following the lockdown and associated risk factors: a multicohort study. Preprint at medRxiv. <https://doi.org/10.1101/2020.09.16.20195693>.
- Rudberg, A.-S., Haverfall, S., Månberg, A., Jernbom Falk, A., Aguilera, K., Ng, H., Gabrielsson, L., Salomonsson, A.-C., Hanke, L., Murrell, B., et al. (2020). SARS-CoV-2 exposure, symptoms and seroprevalence in healthcare workers in Sweden. *Nat. Commun.* 11, 5064. <https://doi.org/10.1038/s41467-020-18848-0>.
- Anand, S., Montez-Rath, M., Han, J., Bozeman, J., Kerschmann, R., Beyer, P., Parsonnet, J., and Chertow, G.M. (2020). Prevalence of SARS-CoV-2 antibodies in a large nationwide sample of patients on dialysis in the USA: a cross-sectional study. *Lancet* 396, 1335–1344. [https://doi.org/10.1016/S0140-6736\(20\)32009-2](https://doi.org/10.1016/S0140-6736(20)32009-2).
- Ward, H., Atchison, C., Whitaker, M., Ainslie, K.E.C., Elliott, J., Okell, L., Redd, R., Ashby, D., Donnelly, C.A., Barclay, W., et al. (2021). SARS-CoV-2 antibody prevalence in England following the first peak of the pandemic. *Nat. Commun.* 12, 905. <https://doi.org/10.1038/s41467-021-21237-w>.
- Buss, L.F., Prete, C.A., Abraham, C.M.M., Mendrone, A., Salomon, T., de Almeida-Neto, C., França, R.F.O., Belotti, M.C., Carvalho, M.P.S.S., Costa, A.G., et al. (2021). Three-quarters attack rate of SARS-CoV-2 in the Brazilian Amazon during a largely unmitigated epidemic. *Science* 371, 288–292. <https://doi.org/10.1126/science.abe9728>.
- Choe, P.G., Kang, C.K., Suh, H.J., Jung, J., Song, K.-H., Bang, J.H., Kim, E.S., Kim, H.B., Park, S.W., Kim, N.J., et al. (2021). Waning antibody responses in asymptomatic and symptomatic SARS-CoV-2 infection. *Emerg. Infect. Dis.* 27, 327–329. <https://doi.org/10.3201/eid2701.203515>.
- Ibarrondo, F.J., Fulcher, J.A., Goodman-Meza, D., Elliott, J., Hofmann, C., Hausner, M.A., Ferbas, K.G., Tobin, N.H., Aldrovandi, G.M., and Yang, O.O. (2020). Rapid decay of anti-SARS-CoV-2 antibodies in persons with mild COVID-19. *N. Engl. J. Med.* 383, 1085–1087. <https://doi.org/10.1056/NEJMc2025179>.
- Long, Q.X., Tang, X.J., Shi, Q.L., Li, Q., Deng, H.J., Yuan, J., Hu, J.L., Xu, W., Zhang, Y., Lv, F.J., et al. (2020). Clinical and immunological assessment of asymptomatic SARS-CoV-2 infections. *Nat. Med.* 26, 1200–1204. <https://doi.org/10.1038/s41591-020-0965-6>.
- Seow, J., Graham, C., Merrick, B., Acors, S., Pickering, S., Steel, K.J.A., Hemmings, O., O'Byrne, A., Kouphou, N., Galao, R.P., et al. (2020). Longitudinal observation and decline of neutralizing antibody responses in the three months following SARS-CoV-2 infection in humans. *Nat. Microbiol.* 5, 1598–1607. <https://doi.org/10.1038/s41564-020-00813-8>.
- Cervia, C., Nilsson, J., Zurbuchen, Y., Valaperti, A., Schreiner, J., Wolfensberger, A., Raebler, M.E., Adamo, S., Weigang, S., Emmenegger, M., et al. (2021). Systemic and mucosal antibody responses specific to SARS-CoV-2 during mild versus severe COVID-19. *J. Allergy Clin. Immunol.* 147, 545–557.e9. <https://doi.org/10.1016/j.jaci.2020.10.040>.
- Emmenegger, M., Kumar, S.S., Emmenegger, V., Malinauskas, T., Buettner, T., Rose, L., Schierack, P., Sprinzl, M.F., Sommer, C.J., Lackner, K.J., et al. (2021). Anti-prothrombin autoantibodies enriched after infection with SARS-CoV-2 and influenced by strength of antibody response against SARS-CoV-2 proteins. *PLoS Pathog.* 17, e1010118. <https://doi.org/10.1371/journal.ppat.1010118>.
- Schneider, M.M., Emmenegger, M., Xu, C.K., Condado Morales, I., Meisl, G., Turelli, P., Zografou, C., Zimmermann, M.R., Frey, B.M., Fiedler, S., et al. (2022). Microfluidic characterisation reveals broad range of SARS-CoV-2 antibody affinity in human plasma. *Life Sci. Alliance* 5, e202101270. <https://doi.org/10.26508/LSA.202101270>.
- Gehlhausen, J.R., Little, A.J., Ko, C.J., Emmenegger, M., Lucas, C., Wong, P., Klein, J., Lu, P., Mao, T., Jaycox, J., et al. (2022). Lack of association between pandemic chilblains and SARS-CoV-2 infection. *Proc. Natl. Acad. Sci. USA* 119, e2122090119. <https://doi.org/10.1073/pnas.2122090119>.

21. Emmenegger, M., Fiedler, S., Brugger, S.D., Devenish, S.R.A., Morgunov, A.S., Ilsley, A., Ricci, F., Malik, A.Y., Scheier, T., Batkita, L., et al. (2022). Both COVID-19 infection and vaccination induce high-affinity cross-clade responses to SARS-CoV-2 variants. *iScience* 25, 104766. <https://doi.org/10.1016/j.isci.2022.104766>.
22. Kryštůfek, R., and Šácha, P. (2019). Increasing the throughput of crystallization condition screens: challenges and pitfalls of acoustic dispensing systems. *MethodsX* 6, 2230–2236. <https://doi.org/10.1016/j.mex.2019.09.030>.
23. Kuleskiy, E., Saarela, J., Turunen, L., and Wennerberg, K. (2016). Precision cancer medicine in the acoustic dispensing era: ex vivo primary cell drug sensitivity testing. *J. Lab. Autom.* 21, 27–36. <https://doi.org/10.1177/2211068215618869>.
24. Song, W., Gui, M., Wang, X., and Xiang, Y. (2018). Cryo-EM structure of the SARS coronavirus spike glycoprotein in complex with its host cell receptor ACE2. *PLoS Pathog.* 14, e1007236. <https://doi.org/10.1371/journal.ppat.1007236>.
25. Tai, W., Zhang, X., He, Y., Jiang, S., and Du, L. (2020). Identification of SARS-CoV RBD-targeting monoclonal antibodies with cross-reactive or neutralizing activity against SARS-CoV-2. *Antivir. Res.* 179, 104820. <https://doi.org/10.1016/j.antiviral.2020.104820>.
26. Fenwick, C., Croxatto, A., Coste, A.T., Pojer, F., André, C., Pellaton, C., Farina, A., Campos, J., Hacker, D., Lau, K., et al. (2021). Changes in SARS-CoV-2 spike versus nucleoprotein antibody responses impact the estimates of infections in population-based seroprevalence studies. *J. Virol.* 95, 018288–20. <https://doi.org/10.1128/JVI.01828-20>.
27. Grinsztajn, L., Semenova, E., Margossian, C.C., and Riou, J. (2021). Bayesian workflow for disease transmission modeling in Stan. *Stat. Med.* 40, 6209–6234. <https://doi.org/10.1002/SIM.9164>.
28. Jiang, C., Wang, Y., Hu, M., Wen, L., Wen, C., Wang, Y., Zhu, W., Tai, S., Jiang, Z., Xiao, K., et al. (2020). Antibody seroconversion in asymptomatic and symptomatic patients infected with severe acute respiratory syndrome coronavirus 2 (SARS-CoV-2). *Clin. Transl. Immunol.* 9, e1182. <https://doi.org/10.1002/cti2.1182>.
29. Guo, L., Ren, L., Yang, S., Xiao, M., Chang, D., Yang, F., Dela Cruz, C.S., Wang, Y., Wu, C., Xiao, Y., et al. (2020). Profiling early humoral response to diagnose novel coronavirus disease (COVID-19). *Clin. Infect. Dis.* 71, 778–785. <https://doi.org/10.1093/cid/cia310>.
30. Long, Q.-X., Liu, B.-Z., Deng, H.-J., Wu, G.-C., Deng, K., Chen, Y.-K., Liao, P., Qiu, J.-F., Lin, Y., Cai, X.-F., et al. (2020). Antibody responses to SARS-CoV-2 in patients with COVID-19. *Nat. Med.* 26, 845–848. <https://doi.org/10.1038/s41591-020-0897-1>.
31. Ganyani, T., Kremer, C., Chen, D., Torneri, A., Faes, C., Wallinga, J., and Hens, N. (2020). Estimating the generation interval for coronavirus disease (COVID-19) based on symptom onset data, March 2020. *Euro Surveill.* 25, 2000257. <https://doi.org/10.2807/1560-7917.ES.2020.25.17.2000257>.
32. Linton, N.M., Kobayashi, T., Yang, Y., Hayashi, K., Akhmetzhanov, A.R., Jung, S.M., Yuan, B., Kinoshita, R., and Nishiura, H. (2020). Incubation period and other epidemiological characteristics of 2019 novel coronavirus infections with right truncation: a statistical analysis of publicly available case data. *J. Clin. Med.* 9, 538. <https://doi.org/10.3390/jcm9020538>.
33. Menges, D., Zens, K.D., Ballouz, T., Caduff, N., Llanas-Cornejo, D., Aschmann, H.E., Domenghino, A., Pellaton, C., Perreau, M., Fenwick, C., et al. (2022). Heterogenous humoral and cellular immune responses with distinct trajectories post-SARS-CoV-2 infection in a population-based cohort. *Nat. Commun.* 13, 4855. <https://doi.org/10.1038/s41467-022-32573-w>.
34. Jeong, E., Ko, K., Oh, S., and Han, H.W. (2017). Network-based analysis of diagnosis progression patterns using claims data. *Sci. Rep.* 7, 15561–15612. <https://doi.org/10.1038/s41598-017-15647-4>.
35. Bader, G.D., and Hogue, C.W.V. (2003). An automated method for finding molecular complexes in large protein interaction networks. *BMC Bioinf.* 4, 2. <https://doi.org/10.1186/1471-2105-4-2>.
36. Almqvist, J., Granberg, T., Tzortzakakis, A., Klironomos, S., Kollia, E., Öhberg, C., Martin, R., Piehl, F., Ouellette, R., and Ineichen, B.V. (2020). Neurological manifestations of coronavirus infections – a systematic review. *Ann. Clin. Transl. Neurol.* 7, 2057–2071. <https://doi.org/10.1002/actn.3.51166>.
37. Varatharaj, A., Thomas, N., Ellul, M.A., Davies, N.W.S., Pollak, T.A., Tenorio, E.L., Sultan, M., Easton, A., Breen, G., Zandi, M., et al. (2020). Neurological and neuropsychiatric complications of COVID-19 in 153 patients: a UK-wide surveillance study. *Lancet Psychiatr.* 7, 875–882. [https://doi.org/10.1016/S2215-0366\(20\)30287-X](https://doi.org/10.1016/S2215-0366(20)30287-X).
38. Buehler, P.K., Zinkernagel, A.S., Hofmaenner, D.A., Wendel Garcia, P.D., Acevedo, C.T., Gómez-Mejía, A., Mairpady Shambat, S., Andreoni, F., Maibach, M.A., Bartussek, J., et al. (2021). Bacterial pulmonary superinfections are associated with longer duration of ventilation in critically ill COVID-19 patients. *Cell Rep. Med.* 2, 100229. <https://doi.org/10.1016/j.xcrm.2021.100229>.
39. Tessitore, E., and Meyer, P. (2020). COVID-19 and cardiovascular disease: what have we learned? *Swiss Med. Wkly.* 150, w20452. <https://doi.org/10.4414/smww.2020.20452>.
40. Petrilli, C.M., Jones, S.A., Yang, J., Rajagopalan, H., O'Donnell, L., Chernyak, Y., Tobin, K.A., Cerfolio, R.J., Francois, F., and Horwitz, L.I. (2020). Factors associated with hospital admission and critical illness among 5279 people with coronavirus disease 2019 in New York City: prospective cohort study. *BMJ* 369, m1966. <https://doi.org/10.1136/bmj.m1966>.
41. Jehi, L., Ji, X., Milinovich, A., Erzurum, S., Merlino, A., Gordon, S., Young, J.B., and Kattan, M.W. (2020). Development and validation of a model for individualized prediction of hospitalization risk in 4, 536 patients with COVID-19. *PLoS One* 15, e0237419. <https://doi.org/10.1371/journal.pone.0237419>.
42. Cummins, L., Ebyarimpa, I., Cheetham, N., Brown, V.T., Brennan, K., and Panovska-Griffiths, J. (2021). Factors associated with COVID-19 related hospitalisation, critical care admission and mortality using linked primary and secondary care data. Preprint at medRxiv. <https://doi.org/10.1101/2021.01.19.20241844>.
43. Jafari, M., and Ansari-Pour, N. (2019). Why, when and how to adjust your P values? *Cell J.* 20, 604–607. <https://doi.org/10.22074/cellj.2019.5992>.
44. Tran, V.-T., Porcher, R., Pane, I., and Ravaud, P. (2022). Course of post COVID-19 disease symptoms over time in the ComPaRe long COVID prospective e-cohort. *Nat. Commun.* 13, 1812. <https://doi.org/10.1038/s41467-022-29513-z>.
45. Kamal, M., Abo Omirah, M., Hussein, A., and Saeed, H. (2021). Assessment and characterisation of post-COVID-19 manifestations. *Int. J. Clin. Pract.* 75, e13746. <https://doi.org/10.1111/IJCP.13746>.
46. Yong, S.J. (2021). Long COVID or post-COVID-19 syndrome: putative pathophysiology, risk factors, and treatments. *Infect. Dis.* 53, 737–754. <https://doi.org/10.1080/23744235.2021.1924397>.
47. Menges, D., Ballouz, T., Anagnostopoulos, A., Aschmann, H.E., Domenghino, A., Fehr, J.S., and Puhan, M.A. (2021). Burden of post-COVID-19 syndrome and implications for healthcare service planning: a population-based cohort study. *PLoS One* 16, e0254523. <https://doi.org/10.1371/journal.pone.0254523>.
48. Ma, Q., Liu, J., Liu, Q., Kang, L., Liu, R., Jing, W., Wu, Y., and Liu, M. (2021). Global percentage of asymptomatic SARS-CoV-2 infections among the tested population and individuals with confirmed COVID-19 diagnosis. *JAMA Netw. Open* 4, e2137257. <https://doi.org/10.1001/jamanetworkopen.2021.37257>.
49. Sah, P., Fitzpatrick, M.C., Zimmer, C.F., Abdollahi, E., Juden-Kelly, L., Moghadas, S.M., Singer, B.H., and Galvani, A.P. (2021). Asymptomatic SARS-CoV-2 infection: a systematic review and meta-analysis. *Proc. Natl. Acad. Sci. USA* 118, e2109229118. <https://doi.org/10.1073/pnas.2109229118>.
50. Ulyte, A., Radtke, T., Abela, I.A., Haile, S.R., Berger, C., Huber, M., Schanz, M., Schwarzmueller, M., Trkola, A., Fehr, J., et al. (2021). Clustering and longitudinal change in SARS-CoV-2 seroprevalence in school children in the canton of Zurich, Switzerland: prospective cohort study of 55 schools. *BMJ* 372, n616. <https://doi.org/10.1136/bmj.n616>.
51. Streeck, H., Schulte, B., Kümmerer, B.M., Richter, E., Höller, T., Fuhrmann, C., Bartok,

- E., Dolscheid, R., Berger, M., Wessendorf, L., et al. (2020). Infection fatality rate of SARS-CoV-2 infection in a German community with a super-spreading event. Preprint at medRxiv. <https://doi.org/10.1101/2020.05.04.20090076>.
52. Bendavid, E., Mulaney, B., Sood, N., Shah, S., Bromley-Dulfano, R., Lai, C., Weissberg, Z., Saavedra-Walker, R., Tedrow, J., Bogan, A., et al. (2021). COVID-19 antibody seroprevalence in Santa Clara County, California. *Int. J. Epidemiol.* 50, 410–419. <https://doi.org/10.1093/ije/dyab010>.
53. Ng, K.W., Faulkner, N., Cornish, G.H., Rosa, A., Harvey, R., Hussain, S., Ulferts, R., Earl, C., Wrobel, A.G., Benton, D.J., et al. (2020). Preexisting and de novo humoral immunity to SARS-CoV-2 in humans. *Science* 370, 1339–1343. <https://doi.org/10.1126/science.abe1107>.
54. Arosio, P., Müller, T., Rajah, L., Yates, E.V., Aprile, F.A., Zhang, Y., Cohen, S.I.A., White, D.A., Herling, T.W., De Genst, E.J., et al. (2016). Microfluidic diffusion analysis of the sizes and interactions of proteins under native solution conditions. *ACS Nano* 10, 333–341. <https://doi.org/10.1021/acsnano.5b04713>.
55. Perez-Saez, J., Lauer, S.A., Kaiser, L., Regard, S., Delaporte, E., Guessous, I., Stringhini, S., Azman, A.S., Serocov-POP Study Group, and Arm-Vernez, I., et al. (2021). Serology-informed estimates of SARS-CoV-2 infection fatality risk in Geneva, Switzerland. *Lancet Infect. Dis.* 21, e69–e70. [https://doi.org/10.1016/S1473-3099\(20\)30584-3](https://doi.org/10.1016/S1473-3099(20)30584-3).
56. Hauser, A., Counotte, M.J., Margossian, C.C., Konstantinoudis, G., Low, N., Althaus, C.L., and Riou, J. (2020). Estimation of SARS-CoV-2 mortality during the early stages of an epidemic: a modeling study in Hubei, China, and six regions in Europe. *PLoS Med.* 17, e1003189. <https://doi.org/10.1371/journal.pmed.1003189>.
57. le Vu, S., Jones, G., Anna, F., Rose, T., Richard, J.B., Bernard-Stoecklin, S., Goyard, S., Demeret, C., Helynck, O., Escriviou, N., et al. (2021). Prevalence of SARS-CoV-2 antibodies in France: results from nationwide serological surveillance. *Nat. Commun.* 12, 3025. <https://doi.org/10.1038/s41467-021-23233-6>.
58. Malani, A., Shah, D., Kang, G., Lobo, G.N., Shastri, J., Mohanan, M., Jain, R., Agrawal, S., Juneja, S., Imad, S., and Kolthur-Seetharam, U. (2021). Seroprevalence of SARS-CoV-2 in slums versus non-slums in Mumbai, India. *Lancet Glob. Health* 9, e110–e111. [https://doi.org/10.1016/S2214-109X\(20\)30467-8](https://doi.org/10.1016/S2214-109X(20)30467-8).
59. Pullano, G., Di Domenico, L., Sabbatini, C.E., Valdano, E., Turbelin, C., Debin, M., Guerrisi, C., Kengne-Kuetché, C., Souty, C., Hanslik, T., et al. (2021). Underdetection of cases of COVID-19 in France threatens epidemic control. *Nature* 590, 134–139. <https://doi.org/10.1038/s41586-020-03095-6>.
60. Quast, I., and Tarlinton, D. (2021). B cell memory: understanding COVID-19. *Immunity* 54, 205–210. <https://doi.org/10.1016/j.immuni.2021.01.014>.
61. Altmann, D.M., and Boyton, R.J. (2020). SARS-CoV-2 T cell immunity: specificity, function, durability, and role in protection. *Sci. Immunol.* 5, eabd6160. <https://doi.org/10.1126/sciimmunol.abd6160>.
62. Cohen, M.E., Eichel, R., Steiner-Birmanns, B., Janah, A., Ioshpa, M., Bar-Shalom, R., Paul, J.J., Gaber, H., Skrahina, V., Bornstein, N.M., and Yahalom, G. (2020). A case of probable Parkinson's disease after SARS-CoV-2 infection. *Lancet Neurol.* 19, 804–805. [https://doi.org/10.1016/S1474-4422\(20\)30305-7](https://doi.org/10.1016/S1474-4422(20)30305-7).
63. Faber, I., Brandão, P.R.P., Menegatti, F., de Carvalho Bispo, D.D., Maluf, F.B., and Cardoso, F. (2020). Coronavirus disease 2019 and parkinsonism: a non-post-encephalitic case. *Mov. Disord.* 35, 1721–1722. <https://doi.org/10.1002/mds.28277>.
64. Méndez-Guerrero, A., Laespada-García, M.I., Gómez-Grande, A., Ruiz-Ortiz, M., Blanco-Palmero, V.A., Azcarate-Diaz, F.J., Rábano-Suárez, P., Álvarez-Torres, E., de Fuenmayor-Fernández de la Hoz, C.P., Vega Pérez, D., et al. (2020). Acute hypokinetic-rigid syndrome following SARS-CoV-2 infection. *Neurology* 95, e2109–e2118. <https://doi.org/10.1212/WNL.00000000000010282>.
65. Bull-Otterson, L., Baca, S., Saydah, S., Boehmer, T.K., Adjei, S., Gray, S., and Harris, A.M. (2022). Post-COVID conditions among adult COVID-19 survivors aged 18–64 and ≥65 Years — United States, March 2020–November 2021. *MMWR Morb. Mortal. Wkly. Rep.* 71, 713–717. <https://doi.org/10.15585/MMWR.MM7121E1>.
66. Nehme, M., Brailard, O., Chappuis, F., Courvoisier, D.S., Kaiser, L., Soccac, P.M., Reny, J.L., Assal, F., Bondolfi, G., Tardin, A., et al. (2022). One-year persistent symptoms and functional impairment in SARS-CoV-2 positive and negative individuals. *J. Intern. Med.* 292, 103–115. <https://doi.org/10.1111/JOIM.13482>.
67. Huang, L., Yao, Q., Gu, X., Wang, Q., Ren, L., Wang, Y., Hu, P., Guo, L., Liu, M., Xu, J., et al. (2021). 1-year outcomes in hospital survivors with COVID-19: a longitudinal cohort study. *Lancet* 398, 747–758. [https://doi.org/10.1016/S0140-6736\(21\)01755-4](https://doi.org/10.1016/S0140-6736(21)01755-4).
68. Sigfrid, L., Drake, T.M., Pauley, E., Jesudason, E.C., Oliaro, P., Lim, W.S., Gillesen, A., Berry, C., Lowe, D.J., McPeake, J., et al. (2021). Long Covid in adults discharged from UK hospitals after Covid-19: a prospective, multicentre cohort study using the ISARIC WHO Clinical Characterisation Protocol. *Lancet Reg. Health. Eur.* 8, 100186. <https://doi.org/10.1016/j.lanep.2021.100186>.
69. Heesakkers, H., Van Der Hoeven, J.G., Corsten, S., Janssen, I., Ewalds, E., Simons, K.S., Westerhof, B., Rettig, T.C.D., Jacobs, C., Van Santen, S., et al. (2022). Clinical outcomes among patients with 1-year survival following intensive care unit treatment for COVID-19. *JAMA* 327, 559–565. <https://doi.org/10.1001/JAMA.2022.0040>.
70. Ballouz, T., Menges, D., Anagnostopoulos, A., Domenghino, A., Aschmann, H.E., Frei, A., Fehr, J.S., and Puhani, M.A. (2022). Natural course of post COVID-19 condition and implications for trial design and outcome selection: a population-based longitudinal cohort study. Preprint at medRxiv. <https://doi.org/10.1101/2022.06.22.22276746>.
71. Kordzadeh-Kermani, E., Khalili, H., and Karimzadeh, I. (2020). Pathogenesis, clinical manifestations and complications of coronavirus disease 2019 (COVID-19). *Future Microbiol.* 15, 1287–1305. <https://doi.org/10.2217/fmb-2020-0110>.
72. Gavriatopoulou, M., Korompoki, E., Fotiou, D., Ntanas-Stathopoulos, I., Psaltopoulou, T., Kastiris, E., Terpos, E., and Dimopoulos, M.A. (2020). Organ-specific manifestations of COVID-19 infection. *Clin. Exp. Med.* 20, 493–506. <https://doi.org/10.1007/s10238-020-00648-x>.
73. Pezzini, A., and Padovani, A. (2020). Lifting the mask on neurological manifestations of COVID-19. *Nat. Rev. Neurol.* 16, 636–644. <https://doi.org/10.1038/s41582-020-0398-3>.
74. Rando, H.M., Bennett, T.D., Byrd, J.B., Bramante, C., Callahan, T.J., Chute, C.G., Davis, H.E., Deer, R., Gagnier, J., Korashy, F.M., et al. (2021). Challenges in defining long COVID: striking differences across literature, electronic health records, and patient-reported information. Preprint at medRxiv. <https://doi.org/10.1101/2021.03.20.21253896>.
75. Aschman, T., Mothes, R., Heppner, F.L., and Radbruch, H. (2022). What SARS-CoV-2 does to our brains. *Immunity* 55, 1159–1172. <https://doi.org/10.1016/j.immuni.2022.06.013>.
76. Schooling, C.M., and Jones, H.E. (2014). Is representativeness the right question? *Int. J. Epidemiol.* 43, 631–632. <https://doi.org/10.1093/IJE/DYT264>.
77. Rothman, K.J., Gallacher, J.E.J., and Hatch, E.E. (2013). Why representativeness should be avoided. *Int. J. Epidemiol.* 42, 1012–1014. <https://doi.org/10.1093/IJE/DYS223>.
78. Grimes, D.A., and Schulz, K.F. (2002). Bias and causal associations in observational research. *Lancet* 359, 248–252. [https://doi.org/10.1016/S0140-6736\(02\)07451-2](https://doi.org/10.1016/S0140-6736(02)07451-2).
79. Ioannidis, J.P.A. (2016). Why most clinical research is not useful. *PLoS Med.* 13, e1002049. <https://doi.org/10.1371/JOURNAL.PMED.1002049>.
80. National SARS-CoV-2 Serology Assay Evaluation Group, Andersson, M., Auckland, K., Baillie, J.K., Barnes, E., Beer, S., Beveridge, A., Bibi, S., Blackwell, L., Borak, M., et al. (2020). Performance characteristics of five immunoassays for SARS-CoV-2: a head-to-head benchmark comparison. *Lancet Infect. Dis.* 20, 1390–1400. [https://doi.org/10.1016/S1473-3099\(20\)30634-4](https://doi.org/10.1016/S1473-3099(20)30634-4).
81. Ebner, D., Aguzzi, A., Burgess-Brown, N., Cornall, R., Crook, D., Emmenegger, M., Eyre, D., Launchbury, M., Ferreira, L.M., Hatch, S., et al. (2021). The Oxford SARS-CoV-2 Immunoassay: High throughput antibody testing developed in an academic/clinical environment. 10.6084/M9.FIGSHARE.13522589.V1.

82. Carpenter, B., Gelman, A., Hoffman, M.D., Lee, D., Goodrich, B., Betancourt, M., Brubaker, M.A., Guo, J., Li, P., and Riddell, A. (2017). Stan: a probabilistic programming language. *J. Stat. Softw.* 76. <https://doi.org/10.18637/jss.v076.i01>.
83. Griessbach, A., Bauer, A., Jörgen Lebet, F., and Grossmann, R. (2022). The concept of general consent in Switzerland and the implementation at the University Hospital Zurich, a cross-sectional study. *Swiss Med. Wkly.* 152, w30159. <https://doi.org/10.4414/SMW.2022.W30159>.
84. Senatore, A., Frontzek, K., Emmenegger, M., Chincisan, A., Losa, M., Reimann, R., Horny, G., Guo, J., Fels, S., Sorce, S., et al. (2020). Protective anti-prion antibodies in human immunoglobulin repertoires. *EMBO Mol. Med.* 12, e12739. <https://doi.org/10.15252/emmm.202012739>.
85. Uyoga, S., Adetifa, I.M.O., Karanja, H.K., Nyagwange, J., Tuju, J., Wanjiku, P., Aman, R., Mwangangi, M., Amoth, P., Kasera, K., et al. (2021). Seroprevalence of anti-SARS-CoV-2 IgG antibodies in Kenyan blood donors. *Science* 371, 79–82. <https://doi.org/10.1126/science.abe1916>.
86. Amorim Filho, L., Szwarcwald, C.L., Mateos, S.d.O.G., Leon, A.C.M.P.d., Medronho, R.d.A., Veloso, V.G., Lopes, J.I.F., Porto, L.C.d.M.S., Chieppe, A., and Werneck, G.L.; Grupo Hemorio de Pesquisa em Covid-19 (2020). Seroprevalence of anti-SARS-CoV-2 among blood donors in Rio de Janeiro, Brazil. *Rev. Saude Publica* 54, 1–10. <https://doi.org/10.11606/s1518-8787.2020054002643>.
87. Slot, E., Hogema, B.M., Reusken, C.B.E.M., Reimerink, J.H., Molier, M., Karregat, J.H.M., IJlst, J., Novotný, V.M.J., van Lier, R.A.W., and Zaaier, H.L. (2020). Low SARS-CoV-2 seroprevalence in blood donors in the early COVID-19 epidemic in the Netherlands. *Nat. Commun.* 11, 5744. <https://doi.org/10.1038/s41467-020-19481-7>.
88. Xu, R., Huang, J., Duan, C., Liao, Q., Shan, Z., Wang, M., Rong, X., Li, C., Fu, Y., and Wang, H. (2021). Low prevalence of antibodies against SARS-CoV-2 among voluntary blood donors in Guangzhou, China. *J. Med. Virol.* 93, 1743–1747. <https://doi.org/10.1002/jmv.26445>.
89. Blutspendedienst. (2021). Admission criteria for blood donors. <https://www.blutspendezurich.ch/spender/ich-will-spenden/>.
90. Blutspendedienst. (2021). Detailed inclusion and exclusion criteria for blood donors. https://www.blutspendezurich.ch/fileadmin/pdf/Formulare/Spender/Fragebogen_01.02.2020/d-Neuspenden-V16.pdf.
91. Stadlbauer, D., Amanat, F., Chromikova, V., Jiang, K., Strohmeier, S., Arunkumar, G.A., Tan, J., Bhavsar, D., Capuano, C., Kirkpatrick, E., et al. (2020). SARS-CoV-2 seroconversion in humans: a detailed protocol for a serological assay, antigen production, and test setup. *Curr. Protoc. Microbiol.* 57, e100. <https://doi.org/10.1002/cpmc.100>.
92. Wrapp, D., Wang, N., Corbett, K.S., Goldsmith, J.A., Hsieh, C.-L., Abiona, O., Graham, B.S., and McLellan, J.S. (2020). Cryo-EM structure of the 2019-nCoV spike in the prefusion conformation. Preprint at bioRxiv. <https://doi.org/10.1101/2020.02.11.944462>.
93. Aricescu, A.R., Lu, W., and Jones, E.Y. (2006). A time- and cost-efficient system for high-level protein production in mammalian cells. *Acta Crystallogr. D Biol. Crystallogr.* 62, 1243–1250. <https://doi.org/10.1107/S0907444906029799>.
94. Emmenegger, M., de Cecco, E., Hruska-Plochan, M., Eninger, T., Schneider, M.M., Barth, M., Tantarini, E., de Rossi, P., Bacioglu, M., Langston, R.G., et al. (2021). LAG3 is not expressed in human and murine neurons and does not modulate α -synucleinopathies. *EMBO Mol. Med.* 13, e14745. <https://doi.org/10.15252/emmm.202114745>.
95. Goodrich, B., Gabry, J., Ali, I., and Brilleman, S. (2020). rstanarm: Bayesian applied regression modeling via Stan. <https://mc-stan.org/rstanarm>.
96. Gelman, A., Carlin, J.B., Stern, H.S., Dunson, D.B., Vehtari, A., and Rubin, D.B. (2013). *Bayesian Data Analysis Third Edit* (CRC Press, Taylor & Francis Group).
97. Piironen, J., and Vehtari, A. (2017). Sparsity information and regularization in the horseshoe and other shrinkage priors. *Electron. J. Statist.* 11, 5018–5051. <https://doi.org/10.1214/17-EJS1337SI>.
98. Bundesamt für Statistik (2016). Ortschaftenverzeichnis der Schweiz - MS-excel version. Ortschaftenverzeichnis der Schweiz - MS-excel version. <https://www.bfs.admin.ch/hub/api/dam/assets/275785/master>.
99. Bundesamt für Landestopografie (2020). Auszug Katalog Geobasisdaten des Bundesrechts. https://map.geo.admin.ch/?layers=ch.swisstopo-vd.ortschaftenverzeichnis_plz&lang=en&topic=ech&bgLayer=ch.swisstopo.pixelkarte-farbe&layers_opacity=0.75.

STAR★METHODS

KEY RESOURCES TABLE

REAGENT or RESOURCE	SOURCE	IDENTIFIER
Antibodies		
Goat anti-human IgG, 1:4000	Jackson	109-035-098; RRID: AB_2337586
Goat anti-human IgA, 1:750	Thermo Fisher Scientific	31417; RRID: AB_228253
Chemicals, peptides, and recombinant proteins		
WT SARS-CoV-2 Spike ECD	Oxford, SGC	N/A
WT SARS-CoV-2 RBD	Oxford, SGC	N/A
WT SARS-CoV-2 NC	AcroBiosystems	NUN-C5227
WT SARS-CoV-2 Spike prefusion ECD	Lausanne, EPFL SV PTECH PTPSP and Zurich, UZH	N/A
WT SARS-CoV-2 RBD	Trenzyme	P2020-001
WT SARS-CoV-2 NSP1	Zurich, ETH	N/A
CMV pp65	Abcam	ab43041
Bovine serum albumin (BSA)	Thermo Fisher Scientific	23209
SARS-CoV (2003) RBD	Yale, New Haven	N/A
Critical commercial assays		
SARS-CoV-2 nucleocapsid test on E801 of the COBAS8000® system	Roche diagnostics	N/A
LIAISON® SARS-CoV-2 chemiluminescence immunoassay	DiaSorin	N/A
SARS-CoV-2 chemiluminescent microparticle immunoassay on an Architect™ analyser	Abbott	N/A
IgA or IgG against the SARS-CoV-2 S1 antigen on DSX™ Automated ELISA System	EUROIMMUN and DYNEX	N/A
High-throughput serology assay in Oxford (under development)	Final version of assay published by The National SARS-CoV-2 Serology Assay Evaluation Group ⁸⁰ and described here. ⁸¹	N/A
Experimental models: Cell lines		
Expi293F cells	Thermo Fisher	A14527
ExpiCHO cells	Thermo Fisher	A29127
Vero E6 cells	ATCC	CRL-1586
Software and algorithms		
Python 3	Python Software Foundation	N/A
R 4.2.0 statistical software	R Core Team	N/A
R Studio 2022.07.1 Build 554	R Studio, PBC	N/A
Stan ⁸²	Stan development team	N/A
Code used in the current study	Zenodo repository ¹	https://doi.org/10.5281/zenodo.7454292
GraphPad	Prism	N/A
Other		
1536-well high-binding ELISA plates (SpectraPlate)	Perkin Elmer	6004500
384-well high-binding ELISA plates (SpectraPlate)	Perkin Elmer	6007500

(Continued on next page)

Continued

REAGENT or RESOURCE	SOURCE	IDENTIFIER
384-well low-binding PP plates	Labcyte/Beckman Coulter	001-14555
ECHO 555 Acoustic Dispenser	Labcyte/Beckman Coulter	N/A
El406 Washer/Dispenser	Biotek	N/A
MultifloFX	Biotek	N/A
Certus Flex dispenser	Fritz Gyger AG	N/A
Microplate Centrifuge	Agilent	G5582AA
PlateLoc thermal microplate sealer	Agilent	G5585BA
XPeel automated plate seal removal	Brooks/Azenta	N/A
EnVision multimode plate reader	Perkin Elmer	2105-0010
Fluidity One-W	Fluidic Analytics	N/A
iBlot 2 Gel Transfer Device	Thermo Fisher	IB21001
Fusion SOLO S imaging system	Vilber	N/A

RESOURCE AVAILABILITY

Lead contact

Further information and requests for resources should be directed to and will be fulfilled by the lead contact, Marc Emmenegger (marc.emmenegger@usz.ch).

Materials availability

Small amounts of the biological samples can be shared if available, upon reasonable request, and if an approval by an ethics committee as well as an MTA is in place.

Data and code availability

- Specific data sets can be shared upon reasonable request and if an approval by an ethics committee as well as a data transfer agreement is in place.
- Code used in this study is publicly available on Zenodo¹ and the DOIs are listed in the [key resources table](#).
- Any additional information required to reanalyse the data reported in this paper is available from the [lead contact](#) upon request.

EXPERIMENTAL MODEL AND SUBJECT DETAILS

Ethics statement

All experiments and analyses involving samples from human donors were conducted with the approval of the ethics committee of the canton Zürich, i.e. Kantonale Ethikkommission Zürich (KEK-ZH-Nr. 2015-0561, BASEC-Nr. 2018-01042, and BASEC-Nr. 2020-01731), in accordance with the provisions of the Declaration of Helsinki and the Good Clinical Practice guidelines of the International Conference on Harmonisation. All human donors and patients included in this study provided a written general or informed consent. The concept and development of the written general consent in the light of technical advancement and the growth of large data and sample repositories, and its distinction to the standard informed consent is nicely elaborated in Griessbach et al.⁸³

Study design and sampling

The seroepidemiological survey of CoV2 infection in the greater area of Zurich is a population-based study to investigate the temporal evolution of seropositivity for CoV2 in two independent cohorts. We made use of surplus plasma samples from inpatients and outpatients admitted to the University Hospital of Zurich (USZ) collected daily (Monday-Friday) and used for population-wide interrogations of the antibody repertoire.⁸⁴ For the CoV2 seroprevalence study, we included 4'379 samples prior to December 2019 (prepan-demic samples) and 51'435 samples from December 2019 to December 2020 (copandemic samples). The criteria for our study to include a sample into the analysis were: (1) The patients' blood was sent to the

Institute of Clinical Chemistry (at USZ), (2) there was enough residual heparin plasma (150 μ L) for the automated generation of a research aliquot, (3) no aliquot from the same patient was already provided within the same month, (4) additional information (age, sex, clinical ward to which patient was admitted) was available. Point (3) led to the exclusion of 415 samples and point (4) to the exclusion of 30 samples for the calculation of the seroestimates. While not being completely representative for the entire population of the canton of Zurich *sensu stricto*, we have selected this patient cohort due to the depth of available medical data that will allow to trace long-term effects of CoV2 infections from a clinical stance. At the same time, many of the hospital patients are among the most susceptible within a population and are thus in need of substantial monitoring.

Similar to others,^{12,85–88} we have investigated CoV2 IgG seroprevalence of a healthy adult population, complementing the hospital patients, in blood donors of the Blood Donation Service of the Canton of Zurich. Overall, 16'291 samples (thereof 1'096 prior to December, 2019) from blood donors who consented to further use of their samples for research were randomly selected every month (on average: 1'170 samples/month from December 2019 to December 2020) and sent from the blood donation service to Neuro-pathology. The criteria to be admitted for blood donation are in line with international standards of blood donation services, see.⁸⁹ Blood donors with a confirmed CoV2 infection are excluded from donating blood for four weeks, following the full remission of symptoms. Blood donors have to be at least 18 years of age, weigh at least 50 kg, and feel healthy. In order to be included for blood donation, donors have not undergone a substantial surgery or pregnancy/birth in the past 12 months, have not been subjected to dental treatments in the past 72 hours, and have not received foreign blood since 01.01.1980. Moreover, the inclusion mandates that blood donors have not been to an area at risk of malaria or another region with a high prevalence of infectious diseases. Blood donors are only admitted if they have not been tattooed or acquired a permanent make-up in the past four months. A positive test for HIV, syphilis, hepatitis C or B leads to a definite exclusion. Additionally, blood donors are excluded if they have had new sexual partners within the last four months and if they display sexual risk behavior. Lastly, donors have not been to the England, Wales, Scotland, Northern Ireland, Isle of Man, Channel Islands, Gibraltar or to the Falkland Islands for more than six months between 1980 and 1996. Blood donors over age 65, until maximally age 75, can continue donating blood if they have donated blood earlier (the last, complication-free donation has to date back no longer than two years) and the health survey does not indicate any particular health risk. The detailed inclusion and exclusion criteria are enumerated here.⁹⁰ In total, 72'250 samples from 54'153 individuals were included in the seroprevalence estimation study. The USZ cohort was characterized by a median age of 55 (IQR: 40–68) years and a female:male ratio of 47:53. The BDS cohort was characterized by a median age of 42 (IQR: 28–54) years and a female:male ratio of 41:59. A cohort used for establishment of the serological assay (TRABI) was characterized by a median age of 62 (52–70) years and a female:male ratio of 37:63. Details are provided in Table 1. 136 individuals previously included in the seroprevalence estimation and part of the USZ collective were included in the follow-up health survey conducted in 2022. This cohort was characterized by a median age of 55 (IQR: 41–66) years and a female:male ratio of 40:60 (see Table 2).

Sample annotation and identification of condition positives

Specimens were denoted according to the following conventions: *prepandemic samples*: samples collected before December 2019; *COVID samples*: samples from patients with clinically and/or virologically confirmed CoV2 infection; *copandemic samples*: any samples collected in December 2019 or thereafter.

Within the entire collective of copandemic samples ($n = 66'630$, after subtraction of the 55 samples from individuals used for assay establishment and not included for the seroprevalence estimation, see Table 1), we identified condition positives, post-hoc, i.e. after performing the high-throughput serological screening. To be considered a condition positive, the following criteria needed to be fulfilled, (a) for USZ: (1) clinically manifest COVID-19 pneumonia and (2) positive RT-qPCR for CoV2 and (3) venipuncture occurring ≥ 14 days after the first positive qPCR to account for seroconversion. (b) for BDS: Blood donors of the BDS with (1) PCR-confirmed CoV2 infection and (2) convalescent survivors of COVID-19 recruited for a plasmapheresis study conducted with blood donors and part of the same pool of BDS samples sent to us for the seroprevalence study. Importantly, while the condition positives from USZ ($n = 78$) are part of the collective used for the estimation of seroprevalence in the USZ sample, the condition positives from BDS ($n = 76$) are not part of the same collective and are not counted for seroprevalence estimation; as mentioned, BDS recruited convalescent donors outside the regular blood donation activities and the

inclusion of specifically recruited COVID-19 survivors would have biased the seroprevalence estimation. The condition positives ($n = 154$), together with the condition negatives ($n = 5'475$) were used for modelling the seroprevalence (see section [QDA, LDA, and prevalence estimation](#)), both for USZ as well as for BDS individually.

METHOD DETAILS

High-throughput serological screening

In order to test the samples for the presence of IgG antibodies directed against CoV2 antigens, high-binding 1536-well plates (Perkin Elmer, SpectraPlate 1536 HB) were coated with 1 $\mu\text{g/mL}$ S or RBD or NC in PBS at 37°C for 1 h, followed by 3 washes with PBS-T (using Biotek EI406) and by blocking with 5% milk in PBS-T (using Biotek MultifloFX peristaltic pumps) for 1.5 h. Three μL plasma, diluted in 57 μL sample buffer (1% milk in PBS-T), were dispensed at various volumes (from 1,200 nL down to 2.5 nL) into pre-coated 1536-well plates using contactless dispensing with an ECHO 555 Acoustic Dispenser (Labcyte/Beckman Coulter). Sample buffer was filled up to 3 μL total well volume using a Fritz Gyger AG Certus Flex dispenser. Thereby, dilution curves ranging from plasma dilutions 1:50 to 1:6000 were generated (eight dilution points per patient plasma sample). After the sample incubation for 2 h at RT, the wells were washed five times with wash buffer and the presence of IgGs directed against above-defined CoV2 antigens was detected using an HRP-linked anti-human IgG antibody (Peroxidase AffiniPure Goat Anti-Human IgG, Fc γ Fragment Specific, Jackson, 109-035-098, at 1:4000 dilution in sample buffer). The incubation of the secondary antibody for one hour at RT was followed by three washes with PBS-T, the addition of TMB, an incubation of three minutes at RT, and the addition of 0.5 M H_2SO_4 (both steps with Biotek MultifloFX syringe technology). The final well volume for each step was 3 μL . The plates were centrifuged after all dispensing steps, except for the addition of TMB. The absorbance at 450 nm was measured in a plate reader (Perkin Elmer, EnVision) and the inflection points of the sigmoidal binding curves were determined using the custom designed fitting algorithm described below. The secondary antibodies we have used were tested and validated previously²¹ and replicability as well as influence of different sample types (e.g. serum and heparin plasma) on the TRABI have already been reported.^{18,21}

Counter screening using commercial and custom-designed platforms

We used the following commercial tests for the detection of anti-CoV2 antibodies in 55 plasma samples of 27 patients who were diagnosed by RT-PCR to be infected by CoV2 as well as 83–90 plasma samples which were collected before December 2019 and, hence, before the start of the COVID-19 pandemics: The double-antigen sandwich electro-chemiluminescence immunoassay from Roche diagnostics (Rotkreuz, Switzerland) was performed with the E801 of the COBAS8000® system (Roche diagnostics, Rotkreuz, Switzerland). The test detects any antibody against the nucleocapsid antigen. The fully automated LIAISON® CoV2 chemiluminescence immunoassay from DiaSorin (Saluggia, Italy) detects IgG against the S1/S2 antigens. The CoV2 chemiluminescent microparticle immunoassay from Abbott (Abbott Park, IL, USA) detects IgG against the nucleocapsid antigen and was performed on an Architect™ analyser. Two ELISAs from EUROIMMUN (Lübeck, Germany) detect IgA or IgG against the S1 antigen and were performed by the use of a DSX™ Automated ELISA System (DYNEX Technologies (Chantilly, VA, USA)). The high-throughput serology assay in Oxford (under development) was carried out in the Target Discovery Institute, University of Oxford. High-binding 384-well plates (Perkin Elmer, SpectraPlate) were coated with 20 μL of 2.5 $\mu\text{g/mL}$ S o/n at 4°C, followed by 3 washes with PBS-T and by blocking with 5% milk in PBS-T for 2 h. Blocking buffer was removed and 20 μL of 1:25 sera diluted in sample buffer (1% milk in PBS-T) was dispensed into S-coated wells then incubated for 2 h at RT. The wells were washed five times with wash buffer and the presence of IgGs directed against S was detected using an HRP-linked anti-human IgG antibody (Peroxidase AffiniPure Goat Anti-Human IgG, Fc γ Fragment Specific, Jackson, 109-035-098) at 1:50,000 dilution in 20 μL sample buffer. The incubation of the secondary antibody for one hour at RT was followed by three washes with PBS-T and the addition of QuantaRed™ Enhanced Chemifluorescent HRP Substrate Kit (Thermo Scientific, Waltham Massachusetts, USA) then incubated for four minutes at RT before the addition of the stop solution. The fluorescence at excitation/emission maxima of ~570/585 nm was measured in a fluorescent plate reader (Perkin Elmer, EnVision).

Protein production

The proteins were produced and purified at different sites in Zurich (CH), Oxford (UK), Lausanne (CH), and Yale University (USA).

Oxford, SGC

Recombinant proteins were purified as reported previously with small modifications.^{91,92} Mammalian expression vectors containing secreted, codon-optimized CoV2 S (pHL-Sec⁹³; aa. 1-1208, C-terminal 8His-Twin-Strep) and RBD (pOPINTTGNeo; aa. 330-532, C-terminal 6His) were transiently transfected with linear PEI into Expi239TM cells cultured in roller bottles in FreeStyle 293 media. Cell culture media was harvested after 3 days at 37°C for RBD or 3 days at 30°C for Spike and then buffered to 1X PBS. Proteins were first pulled down on Ni²⁺ IMAC Sepharose® 6 Fast Flow (GE) with stringent washing (>50 CV with 40 mM imidazole). RBD was polished on a Superdex 75 16/600 column (GE) equilibrated with 1X PBS, while Spike was directly dialyzed into 1X PBS using SnakeSkinTM 3,500 MWCO dialysis tubing. Proteins were concentrated with VivaSpin® centrifugal concentrators, centrifuged at 21,000 × g for 30 min to remove precipitates, and flash frozen at 1 mg/mL.

Lausanne, EPFL SV PTECH PTPSP and Zurich UZH

The prefusion ectodomain of the CoV2 S protein (the construct was a generous gift from Prof. Jason McLellan, University of Texas, Austin; see⁹²) was transiently transfected either into suspension-adapted ExpiCHO cells (Thermo Fisher) or Expi293F (Thermo Fisher) cells with PEI MAX (Polysciences) in ProCHO5 medium (Lonza). After transfection, incubation with agitation was performed at 31°C and 4.5% CO₂ for 5 days. The clarified supernatant was purified in two steps; via a Strep-Tactin XT column (IBA Lifesciences) followed by Superose 6 10/300 GL column (GE Healthcare) and finally dialyzed into PBS. The average yield was 15 mg/L culture.

Yale, New Haven

Human codon optimized SARS-CoV (2003) RBD (pEZT containing H7 leader sequence; aa. 306-527, C-terminal Avi- and 8His tags) was transiently transfected into Expi293TM cells (Thermo Fisher) using the ExpiFectamineTM 293 Transfection kit (Gibco) according to the manufacturer's instructions. Cells were cultured in a 37°C incubator with 8% humidified CO₂ for 4 days after transfection. Culture supernatant was collected by centrifugation (500 × g for 10 minutes) and RBD was captured using Ni-NTA Superflow resin (Qiagen), washed, and eluted in buffer containing 50 mM Tris-HCl pH 8, 350 mM NaCl, and 250 mM imidazole. RBD was further purified using an ENrichTM SEC 650 column (Bio-Rad) equilibrated in 1X PBS (Thermo Fisher). Peak fractions were pooled and the protein concentration was determined by 280 nm absorbance with a NanodropTM One Spectrophotometer (Thermo Fisher). Protein was snap frozen in liquid nitrogen and shipped on dry ice prior to experiments.

Zurich, ETH

NSP1 carrying an N-terminal His₆-tag followed by a TEV cleavage site was expressed from a pET24a vector. The plasmid was transformed into *E. coli* BL21-CodonPlus (DE3)-RIPL and cells were grown in 2xYT medium at 30°C. At an OD₆₀₀ of 0.8, cultures were shifted to 18°C and induced with IPTG to a final concentration of 0.5 mM. After 16 h, cells were harvested by centrifugation, resuspended in lysis buffer (50 mM HEPES-KOH pH 7.6, 500 mM KCl, 5 mM MgCl₂, 40 mM imidazole, 10% (w/v) glycerol, 0.5 mM TCEP and protease inhibitors) and lysed using a cell disrupter (Constant Systems Ltd). The lysate was cleared by centrifugation for 45 min at 48,000 xg and loaded onto a HisTrap FF 5-mL column (GE Healthcare). Eluted proteins were incubated with TEV protease at 4°C overnight and the His₆-tag, uncleaved NSP1 and the His₆-tagged TEV protease were removed on the HisTrap FF 5-mL column. The sample was further purified via size-exclusion chromatography on a HiLoad 16/60 Superdex75 (GE Healthcare), buffer exchanging the sample to the storage buffer (40 mM HEPES-KOH pH 7.6, 200 mM KCl, 40 mM MgCl₂, 10% (w/v) glycerol, 1 mM TCEP). Fractions containing NSP1 were pooled, concentrated in an Amicon Ultra-15 centrifugal filter (10-kDa MW cut-off), flash-frozen in liquid nitrogen, and stored until further use at -80°C.

Details of viral proteins used for this study

For high-throughput serology, the following proteins were used: CoV2 S (pHL-Sec; aa. 1-1208, C-terminal 8His-Twin-Strep) and RBD (pOPINTTGNeo; aa. 330-532, C-terminal 6His) produced at the SGC in Oxford and the nucleocapsid protein from AcroBiosystems (AA Met 1 - Ala 419, C-terminal his-tag, NUN-C5227). For competitive ELISA, we used: The prefusion ectodomain of the CoV2 S protein (Lausanne, EPFL SV PTECH PTPSP), the RBD from Trenzyme (C-terminal his-tag, P2020-001) and the nucleocapsid protein from AcroBiosystems (AA Met 1 - Ala 419, C-terminal his-tag, NUN-C5227). For additional ELISAs following the high-throughput serology, we used: The prefusion ectodomain of the CoV2 S protein (Lausanne, EPFL

SV PTECH PTPSP), the RBD from Trenzyme (C-terminal his-tag, P2020-001), the nucleocapsid protein from AcroBiosystems (AA Met 1 - Ala 419, C-terminal his-tag, NUN-C5227), the CoV2 NSP1 protein (from Nenad Ban, ETH Zurich), the CMV pp65 protein (Abcam, ab43041), and BSA (Thermo Scientific).

Assay validation

High-throughput validation screen

For the validation screen, we picked 60 and 150 samples from BDS and USZ, respectively, that had the high average values when summing $-\log EC_{50}$ for both Spike and RBD. Additionally, we added 52 and 70 randomly selected prepandemic samples for the BDS and the USZ cohort respectively. We supplemented the three antigens used in the first screen (NC, S, RBD of SARS-CoV2) with a SARS-CoV RBD antigen. Unlike for the primary screen, we ran all samples in duplicates spread over two independent plates.

Western blotting

Expi293F cells were obtained as a gift from Prof. Maurizio Scaltriti (Memorial Sloan Kettering Cancer Center, New York). Non transfected control cells and cells overexpressing either His-tagged S, His-tagged NC or His-tagged RBD domain were lysed in 0,1% Triton X-100/PBS. Total protein content in the cellular fraction was quantified using bicinchoninic protein assay (Pierce BCA Protein Assay Kit, ThermoFisher). For Western Blotting, 30 μ g of ECD-expressing lysate, 10 μ g of NC-expressing lysate and 10 μ g of RBD-expressing lysate were loaded all in the same well of NU-PAGE 4–12% Bis-Tris gels (ThermoFisher). 50 μ g of non-transfected cell lysate were loaded as negative control. Gels were run at a constant voltage (150 V) in MES running buffer for 50 minutes, then transferred onto PVDF membrane with a dry transfer system (iBlot 2 Gel Transfer Device, ThermoFisher). The membranes were blocked with 5% SureBlock (Lubio Science) for 1 hour at room temperature, and then incubated overnight with a 1:100 dilution of patients' plasma in 1% SureBlock, at 4 degrees. The day after, membranes were washed four times with PBS-T and incubated for 1 hours with an anti-human secondary antibody, HRP-conjugated, diluted 1:10000 in 1% SureBlock. The membranes were then washed four times with PBS-T and acquired using Immobilon Crescendo HRP Substrate (Merck Millipore) and Fusion SOLO S imaging system (Vilber). As a positive control, one membrane was incubated overnight with mouse anti-His-tag antibody (ThermoFisher, dilution 1:10000 in 1% SureBlock) and subsequently with anti-mouse secondary antibody, HRP-conjugated (Jackson, dilution 1:10000 in 1% SureBlock).

384-Well ELISA using multiple antigens

High-binding 384-well plates (Perkin Elmer, SpectraPlate 384 HB) were coated with 20 μ L 1 μ g/mL WT SARS-CoV-2 S (Lausanne, EPFL SV PTECH PTPSP), RBD (Trenzyme), NC (AcroBiosystems), BSA (ThermoScience), CMV pp65 (abcam, #ab43041), or NSP1 (Zurich, ETH) in PBS at 37°C for 1 h, followed by 3 washes with PBS 0.1% Tween-20 (PBS-T) using Biotek EI406 and by blocking with 40 μ L 5% milk in PBS-T for 1.5 h. Serum samples were diluted in sample buffer (1% milk in PBS-T) and a serial dilution (range: $0.005-3 \times 10^{-7}$) was carried out (volume: 20 μ L/well). After the sample incubation for 2 h at RT, the wells were washed five times with wash buffer and the presence of IgGs or IgAs directed against above-defined antigens was detected using an HRP-linked anti-human IgG antibody (Peroxidase AffiniPure Goat Anti-Human IgG, Fc γ Fragment Specific, Jackson, 109-035-098, at 1:4000 dilution in sample buffer) or HRP-linked anti-human IgA antibody (Goat anti-Human IgA (Heavy chain) Secondary Antibody, HRP, 31417, ThermoFisher Scientific, at 1:750 dilution in sample buffer), 20 μ L/well. The incubation of the secondary antibody for one hour at RT was followed by three washes with PBS-T, the addition of TMB, an incubation of five minutes at RT, and the addition of 0.5 M H₂SO₄. The plates were centrifuged after all dispensing steps, except for the addition of TMB. The absorbance at 450 nm was measured in a plate reader (Perkin Elmer, EnVision) and the inflection points of the sigmoidal binding curves (pEC_{50} values of the respective sample dilution) were determined using the custom designed fitting algorithm referred to earlier. The pEC_{50} values for all samples and antigens was visualized using the ggplot2 package in R. The HRP-linked antibodies used have previously been validated in depth, see.²¹

Competitive ELISA

To perform competitive ELISAs, high-binding 384-well plates (Perkin Elmer, SpectraPlate 384 HB) were coated with 1 μ g/mL S or RBD or NC in PBS at 37°C for 1 h, followed by 3 washes with PBS-T and by blocking with 5% milk in PBS-T for 1.5 h. Meanwhile, plasma samples were diluted to a final concentration close to

the EC₅₀, incubated with either RBD (50 µg/mL) or S (12.5 µg/mL) and serially diluted (11 dilution points per patient sample, 25 µL per dilution) in low-binding 384-well plates (Labcyte 384 PP plates). After 2 h of incubation at RT, 20 µL of all the samples were transferred to the previously coated plates and incubated for additional 2 h at RT. Then, the plates were washed five times with PBS-T and the presence of IgGs was detected using an HRP-linked anti-human IgG antibody (Peroxidase AffiniPure Goat Anti-Human IgG, Fcγ Fragment Specific, Jackson, 109-035-098, at 1:4000 dilution in sample buffer). The incubation of the secondary antibody for one hour at RT was followed by three washes with PBS-T, the addition of TMB, an incubation of 5 minutes at RT, and the addition of 0.5 M H₂SO₄. The absorbance at 450 nm was measured in a plate reader (Perkin Elmer, EnVision). Data were interpreted and the following qualitative categories were assigned: (1) No binding to target protein, no competition. (2) Binding to target protein, no competition. (3) Binding to target protein, competition.

Microfluidic diffusional sizing

For the microfluidic binding measurements, 40% of human plasma was added to 10 nM antigen and PBS was added to give a constant volume of 20 µL. The antigen used was RBD labelled with Alexa Fluor 647 through N-terminal amine coupling. These samples were incubated at room temperature for 40 minutes and the size, hence molecular weight of the formed immunocomplex, was determined through measuring the hydrodynamic radius, R_h , with microfluidic diffusional sizing^{19,21,54,94} using a Fluidity One-W platform (Fluidic Analytics, Cambridge, UK). Following correction of fluorescence intensities for serum autofluorescence, the fraction, f_d , of RBD to diffuse into the distal channel is defined by:

$$f_d = \frac{[AbR](1 - \rho_b) + ([R]_0 - [AbR])(1 - \rho_f)}{[R]_0}$$

Where $[AbR]$ is the concentration of bound RBD, $[R]_0$ is the total concentration of RBD, and ρ_b and ρ_f are the fractions of bound and free RBD to diffuse into the distal channel, respectively.

QUANTIFICATION AND STATISTICAL ANALYSIS

Analysis of data derived from high-throughput serological screen

Data fitting

Eight-dilution points equally spaced on a logarithmic scale are fitted with an equation derived from a simple binding equilibrium. The inflection point ($-\log_{10}EC_{50}$) is extracted from the fit. Baseline and plateau values are fixed by the respective positive and negative controls in a plate-wise fashion and the signal is fitted following these equations:

$$c_{bound} = 1 - \frac{1}{2} \left(c_a c + k_d + 1 - \sqrt{(c_a c + k_d)^2 + 2(k_d - c_a c) + 1} \right),$$

where c_{bound} , c_a and c are concentration of the antigen-antibody, antigen, and blood concentration respectively.

$$OD_{signal} = c_{bound} (baseline - plateau) + plateau$$

Data preprocessing

Imagine a sample whose physical dilutions (from 1:50 to 1:6'000) do not show deviations in measured signal, i.e. are a straight line in the range of the negative control (absence of antibody binding independent of the dilution). The data fitting process enforces a sigmoid onto the data, resulting in a $-\log_{10}EC_{50}$ value, no matter what the actual shape of the data might be. $-\log_{10}EC_{50}$ values derived from near-straight lines are biologically meaningless when being three orders of magnitude above the non-diluted sample. Importantly, while this means that no samples/values were excluded from seroprevalence measurement, samples for which one or multiple (against S and/or against RBD and/or against NC) $-\log_{10}EC_{50}$ values were below 3 automatically had a posterior probability of 0. This approach was cross-validated by rescaling the $-\log_{10}EC_{50}$ values of affected samples to 0, yielding a posterior probability of <0.1 in all instances. In total 82'130 $-\log_{10}EC_{50}$ values were categorized as such. None of these sample has been used to train the QDA- or LDA-based TRABI model. Importantly, this means that no samples/values were excluded from seroprevalence measurement but that samples for which one or multiple $-\log_{10}EC_{50}$ values were below 3 had a posterior probability of 0.

QDA, LDA, and prevalence estimation

Assume that we have data for m samples with known serostatus and antibody measurements, that is, we have $(X_i, Y_i), i = 1, \dots, m$, where X_i is the vector of size p (in our case our antigen measurements) and Y_i is a Boolean variable defining group membership (in our case, whether the individual is seropositive or not). The QDA model assumes multivariate normal distributed X_i given Y_i :

$$(X|Y = j) \sim \mathcal{N}_p(\mu_j, \Sigma_j),$$

where $j = 0, 1$ is indexing the seropositivity state. Further, the model assumes that the prior, that is, distribution of Y_i , is known s. t. $P[Y = j] = \pi_j$. The quadratic discriminant classifier simply assigns each sample to the group which has the larger posterior $P[Y|X]$, which is proportional to the joint probability $P[Y, X]$. Therefore, we assign sample i to group 1 if

$$\log(f_{x|y=1}(x_i)) + \log(\pi_1) > \log(f_{x|y=0}(x_i)) + \log(\pi_0),$$

and to group 0 otherwise. To set the prior, one option is to take the proportion of serostatus group membership in the dataset for which serostatus is known. However, this is not an ideal option in our case, where we have an additional n samples with unknown serostatus to classify: The prevalence in the m samples with known serostatus might deviate substantially from the prevalence in population with unknown serostatus. We therefore estimate π_1 directly from the data of unknown serostatus using a simple expectation maximization scheme. Proceeding in an iterative fashion, from a given estimate π_1^k , we define the posterior (E step):

$$t_1^k(x_i) = \frac{\pi_1^k f_{x|y=1}(x_i)}{\pi_1^k f_{x|y=1}(x_i) + (1 - \pi_1^k) f_{x|y=0}(x_i)}.$$

Then, we update our estimate of π_1 (M step):

$$\pi_1^{k+1} = \sum_{i=1}^m \frac{t_1^k(x_i)}{m},$$

where m is the number of samples, i.e. the updated seropositive proportion prior is the average of the current estimates of posterior probabilities to be seropositive. After convergence, this yields our estimate of the positive serostatus prevalence in the samples. Note that the sample ordering according to this classifier is independent of the prior and therefore has no impact on an analysis via ROC curves. Further, note that evaluating QDA via ROC analysis, an out of sample scheme should be employed to avoid biased estimates of performance; we chose 10-fold cross-validation throughout, where the samples with known seropositivity status were split in 10 folds ensuring that known/condition positive and negative samples were distributed evenly across the folds. For each fold, the model was fitted on the data in the 9 remaining folds (and the data with unknown seropositivity status to derive the priors). Then, the estimated model parameters were applied to estimate the posterior probabilities of the samples in the left-out fold. Lastly, note that the strategy does not critically depend on the normality assumption but just requires an estimate for the density functions, $f_{x|y=j}(x_i)$. Even nonparametric estimates could be an option.

For the LDA approach, we first collapse the antigen measurements per samples according to the linear discriminant classifier:

$$z_i = x_i^T \Sigma_0^{-1}(\mu_1 - \mu_0),$$

Where Σ_0 is the covariance estimated from the known negatives only and μ_1, μ_0 are the means of the known positives (condition positives) and known negatives (condition negatives) respectively. The above algorithm is then applied on the resulting one dimensional variable z_i . 95% confidence intervals were derived by bootstrap drawing 1,000 bootstrap samples, where the number of samples drawn from each annotation group (known positives/condition positives, known negatives/condition negatives and unannotated) was kept constant. All available known seronegative (i.e. pre-pandemic), known seropositive and samples with unknown serostatus were used in bootstrapping (see Table 1 for detailed listing).

Epidemiological modelling

Post-stratification of age and sex with distributional information of population of canton of Zurich

We adjusted the estimates for differences in age and sex between the population of the canton of Zurich and the samples of individuals hospitalized at UZH or blood donors using inverse probability weighting.

The data for the population of the canton of Zurich were obtained from the statistical services of the canton of Zurich.

Antibody waning and cumulative incidence

Without presuming the effects of antibody waning on immunity to CoV2 re-infection, it is important to account for it when estimating the infection attack rate or cumulative incidence from seroprevalence data. To this aim, we propose an extension to the classic SEIR model where the R compartment (R for removed) in the classical formulation is split in 3: (1) Compartment R represents the subgroup of population that is removed from infectiousness and did not seroconvert yet. (2) Compartment A (for antibody) represents the subgroup of population that is removed from infectiousness and did seroconvert. (3) Compartment W (for waning) represents the subgroup of population that is removed from infectiousness and whose antibodies waned. The model thus assumes the following form:

$$S \xrightarrow{\beta(t)SI} E \xrightarrow{\sigma E} I \xrightarrow{\gamma I} R \xrightarrow{\lambda R} A \xrightarrow{\tau A} W,$$

where S stands for susceptible, E for exposed, I for infectious, and β , σ , γ , λ , and τ are rates. We select a rate λ of 1/14 days for seroconversion (14 days on average from R to A, see^{28–30}), and estimate the rate of antibody waning (τ) from data. The model also assumes an average generation interval of 5.2 days,³¹ and an average time from disease onset to death of 20.2 days.³² We include a time-varying transmission factor by month, $\beta(t)$, with smooth transitions handled by logistic switch functions. The model is fitted to seroprevalence data from USZ and BDS jointly, and to weekly mortality data from canton of Zurich with an infection fatality ratio fixed over time with a prior distribution set to 0.5% (95% central range: 0.2 to 1.0%).⁵⁶ The model was fitted in a Bayesian framework using Stan,⁸² by which the 95% credible intervals were computed through MCMC sampling. From the fitted model we can estimate the rate of antibody waning (or its half-life, i.e. $\log(2)/\tau$, in days) as well as the infection attack rate/cumulative incidence corrected for antibody waning at any time point ($1-S(t)$), see Figure 3E. We additionally investigated antibody decay longitudinally. Over the study period, 65 individuals with a posterior probability of seropositivity above 0.5 had a second measure of SARS-CoV-2 antibodies later. We used a hierarchical linear regression model in Stan to assess the decrease of each $-\log_{10}(EC_{50})$ S, RBD, NC, and the compound QDA-based posterior measurement (on the logit scale), see Figure 3D.

Exploratory correlation analysis of CoV2 seropositivity with ICD-10 codes using Bayesian logistic regression

We explored associations between the posterior probability of a positive serology in individuals consulting at USZ and medical conditions as measured by the ICD-10 codes entered by the medical encoders for health insurance-related purposes. Whenever available, ICD-10 codes were extracted from our clinical data warehouse for all patients included in this study. Up to 100 different ICD-10 codes per case were annotated in a pivot table. We considered only the highest posterior probability for patients with multiple samples (some of which may be negative in the beginning and turn positive later on), and ICD-10 codes entered at any point. We limited the analysis to ICD-10 codes present in more than 0.1% of cases, to avoid overinterpretation of rare events. The analysis was thus focused on 37'382 individuals and 199 variables, including age, sex and 197 ICD-10 codes. We used multiple logistic regression after logit-transforming the posterior probability. We placed ourselves in a Bayesian framework and conduct the analyses in the R package rstanarm.⁹⁵ We started with standard regression, using uninformative priors on regression coefficients (Normal(0,10)). With this large number of covariates, the estimates were, as expected, very noisy and basically unusable. We thus used regularization techniques (Bayesian LASSO and regularized horse-shoe priors, see^{96,97}). We then showed the top ten positive or negative associations between ICD-10 codes and posterior probability of CoV2 seropositivity (odds ratio with 95% credible interval), see Figure 5.

Investigation of feature dissimilarity between seropositive and seronegative patients using linear and nonlinear dimensionality reduction mechanisms

The same dataset as described above (Bayesian logistic regression) was subjected to dimensionality reduction, with the following deviations: (1) Age was not included as a feature. (2) Seropositivity was defined as posterior probability ≥ 0.5 . PCA. PCA was carried out using the default implementation in the R stats package (prcomp) and data was visualized using the factoextra package (<https://cran.r-project.org/web/packages/factoextra/index.html>). UMAP. The following UMAP configuration parameters from the umap package in R (<https://CRAN.R-project.org/package=umap>) were used, all of which are default, except

for the metric where cosine was used instead of Euclidean due to the binary nature of the data (n_neighbors: 15, n_components: 2, metric: cosine, n_epochs: 200, input: data, init: spectral, min_dist: 0.1, set_op_mix_ratio: 1, local_connectivity: 1, bandwidth: 1, alpha: 1, gamma: 1, negative_sample_rate: 5, a: NA, b: NA, spread: 1, random_state: NA, transform_state: NA, knn: NA, knn_repeats: 1, verbose: FALSE, umap_learn_args: NA). UMAP data was plotted using ggplot2 in R. The plots are shown in [Figure S8](#).

Exploratory network analysis of ICD-10 codes, clinical departments, age, and sex for seropositive and seronegative patients

Topological networks have been constructed using the Cytoscape version 3.8.2 (<https://cytoscape.org>), to visualize the patient-ICD-10 code relationship on the network level³⁴ and topological similarities between seropositive and seronegative USZ patients have been scored using the Mcode algorithm.³⁵ ICD-10 codes were depicted as purple rectangles, male patients as diamonds and female patients as circles. The serological status is encoded in red (seropositive) and blue (seronegative), see [Figure S8](#). A force directed layout was employed to represent the network.

Assessing potential complications of CoV2 infection in three patient groups using ICD-10 codes and free-text medical reports

Reports on complications of CoV2 infections beyond the classical COVID-19 pneumonia have accumulated over the past years. To investigate whether a CoV2 infection is associated with diseases that have not been linked to the virus so far, we first split our dataset into (1) seropositive COVID-19 patients hospitalized in the Infectious Diseases or Internal Medicine units (n = 240, group I), (2) seropositive patients associated with other clinical wards (n = 494, group II), and (3) randomly selected seronegative patients (n = 635, group III). Group I likely reflects the cases hospitalized because of COVID-19, while group II is comprised of USZ patients that likely did not require hospitalization due to COVID-19 and some of the patients in this group may have been asymptomatic or paucisymptomatic. Our SQL databases containing ICD-10 codes and free-text medical reports were then queried individually for the three groups, using the following disease classes/conditions: 1) CoV2-related diseases. ICD-10 codes: J80, U69.0-!, J96%. Free text: ARDS, COVID-19-Pneumonie, respiratorische Insuffizienz, Dyspnoe, Lungenembolie. 2) Risk factors for severe disease/hospitalization.^{40–42} Free-text: Diabetes mellitus, Diabetes, Obesity, Herz-Kreislauf, Obesität, Hypertonie, COPD, Arrhythmie, Arrhythmia, chronische Nierenerkrankung, ischämische, Übergewicht, chronische Atemwegserkrankung, Bluthochdruck, Herzfehler, Herzversagen, chronic kidney disease. 3) Mixed neurological/neuropsychiatric.³⁶ Free-text: Fatigue, Müdigkeit, Geschmack, Geruch, Verwirrung, Schwindel, Mood, Psychose, Enzephalitis, microbleed, Schlaganfall, Enzephalopathie, Delir, Epilepsie. 4) Extrapyrimal and movement disorders, therein Parkinson's Disease. ICD-10: G20, G21, G22, G23, G24, G25, G26. Free-text: Parkinson, Dystonie, extrapyramidal, Chorea. 5) Inflammatory diseases of the central nervous system, therein encephalitis. ICD-10: G00, G01, G02, G03, G04, G05, G06, G07, G08, G09. Free-text: Enzephalitis, Enkephalitis, Enzephalomyelitis, Phlebitis, Meningitis, Myelopathie. 6) Demyelinating diseases of the central nervous system, therein multiple sclerosis. ICD-10: G35, G36, G37. Free-text: Multiple Sklerose, Demyelinisation, Demyelinisierung, Hirnsklerose. 7) Hypertensive diseases. ICD-10: I10, I11, I12, I13, I15. Free-text: essentielle Hypertonie, Bluthochdruck, Hypertensive Herzkrankheit, Hypertensive Nierenkrankheit. 8) Ischemic heart diseases. ICD-10: I20, I21, I22, I23, I24, I25. Free-text: Angina pectoris, Myokardinfarkt, ischämische Herzkrankheit. 9) Pulmonary heart disease and diseases of pulmonary circulation. ICD-10: I26, I27, I28. Free-text: Lungenembolie, Lungeninfarkt, pulmonale Herzkrankheit, Thromboembolie. 10) Other forms of heart disease. ICD-10: I30, I31, I32, I33, I34, I35, I36, I37, I38, I39, I40, I41, I42, I43, I44, I45, I46, I47, I48, I49, I50, I51, I52. Free-text: Perikarditis, Perikarderguss, Endokarditis, Mitralklappenkrankheit, Pulmonalklappenkrankheit, Trikuspidalklappenkrankheiten, Pulmonalklappenkrankheiten, Kardiomyopathie, Atrioventrikulärer Block, kardiale Erregungsleitungsstörungen, Herzstillstand, Paroxysmale Tachykardie, Vorhofflimmern, kardiale Arrhythmie, Herzinsuffizienz. 11) Cerebrovascular diseases. ICD-10: I60, I61, I62, I63, I64, I65, I66, I67, I68, I69. Free-text: Subarachnoidalblutung, Intrazerebrale Blutung, Schlaganfall, Aneurysma, Hämorrhagie. 12) Diseases of arteries. ICD-10: I70, I71, I72, I73, I74, I77, I78, I79. Free-text: Aortenaneurysma, periphere Gefäßkrankheiten, Arterielle Embolie und Thrombose. 13) Diseases of veins. ICD-10: I80, I81, I82, I83, I85, I86, I87, I88, I89. Free-text: Thrombophlebitis, Pfortaderthrombose, sonstige venöse Embolie und Thrombose, Ösophagusvarizen, Varizen, Sonstige Venenkrankheiten, Lymphadenitis, Krankheiten der Lymphgefäße und Lymphknoten. 14) Other and unspecified disorders of the circulatory system. ICD-10: I95, I97, I98, I99. Free-text: Hypotonie. The entries were then inspected and multiple entries per patient for a single disease class/condition were reduced into a single entry, to avoid overrepresentation of a single patient. The number of occurrences of unique

patients per disease class/condition were then counted and assembled in a contingency table, with number of patients present for a given disease class/condition and with number of patients absent for a given disease class, for the three groups. Pairwise comparisons were then carried out whereby the data distribution of group I was compared to group II, group I to group III, and group II to group III, for above disease classes/conditions as well as for sex. This resulted in overall 3 x 15 comparisons. Statistical testing was performed using Fisher's exact test, with significance α at 0.01. p-values ≤ 0.01 were then corrected for multiple comparison using p-value adjustment⁴³ where the p-value was multiplied by the number of comparisons performed (i.e. 45). Statistical testing of age was performed using Mann-Whitney U test in GraphPad Prism. Data was visualized with GraphPad Prism as frequencies, i.e. the number of occurrence divided by the total number for each group and each disease class/condition.

Mapping the evolution of seroprevalence in two waves according to municipality in the canton of Zurich

The maps of the canton of Zurich were produced using zip code (PLZ) information of the USZ patients (based on their residency) binned by month for purposes to conserve anonymity. The seroprevalence map (Figures 4C and 4D) displays the ratio of positive versus negative patient samples for each zip code in a given time trace. A threshold of minimally 50 samples per zip code was set in order to minimize statistical fluctuations due to under-sampling a region. This threshold of 50 samples has been made arbitrarily as a tradeoff between the representativity for each zip code and having enough municipalities to represent the sample provenance within the canton of Zurich. In addition, and in order to be able to evaluate any discrepancy, a second map displaying the number of samples analyzed per zip code (independent of seropositivity) has been created (Figures 4A and 4B). The representation of the first six and last six months of the year 2020 has been made in order to compare the evolution of the distribution of seropositivity in the canton of Zurich, between the first and second wave. However, the maps may display significantly lower values than at the seroprevalence peaks as they are averaged over several months. Moreover, we have considered grouping the zip codes together to overcome the limitation of minimally 50 samples per zip code. However, the choice of groups is not trivial, and creates another new bias. The most obvious choice would be to employ a similar population per area but this solution is not straightforward as the population data is provided for municipalities, and not by a zip code. Nevertheless, a second map consisting of arbitrary groups of zip codes has been made in order to make sure we will not miss important information stemming from rural low-number areas (see Figure S7E). The border of the area of the city of Zurich is surrounded by a dense red line while the zip codes contained within the canton of Zurich, at the border to another canton, is displayed with a lighter orange line. Limitation of the zip code as representation of the canton of Zurich: A single unique zip code in Switzerland can be shared between several cantons. As the information collected are represented by the zip code, the map generated can partially include municipalities that belong to a canton other than Zurich. These parts are small, however, except for two regions (Baar, Neuhausen am Rheinfall). These two regions contain an urban area belonging to cantons other than Zurich (Zug, Schaffhausen respectively) and most likely do not solely represent the Zurich area assigned to this zip code. The following document from the Swiss federal statistical office⁹⁸ has been used to find the zip code corresponding to the canton of Zurich; the zip codes 5462 and 8363 have been manually added in order to complete the zip code corresponding to the canton of Zurich. The geographical borders corresponding to the zip code border has been taken from the Swiss federal office of topology swisstopo.⁹⁹ We have moreover calculated the averaged seropositivity rate of the city of Zurich (its boundaries are outlined in red in Figure 4 and in Figure S7E) and the regions of the Canton not within the city limits (outside the zone framed in red colour, see Figure 4) binned by 3 months and evaluated the ratio between them (see Figure S7D). The analyses and the visualization were conducted in Python.

Online health survey

The online health survey was conducted using electronic questionnaires through the REDCap software (<https://www.project-redcap.org/>). The survey questions are provided here¹ within the codebook; they include questions related to specific symptoms experienced in the 7 days prior to completing the questionnaire, relative health status, the EuroQol 5-dimension 5-level (EQ-5D-5L) and the EuroQol visual analogue scale (EQ VAS) instruments. To calculate EQ-5D-5L health state scores, the value set of the Netherlands was applied in lack of a corresponding value set from Switzerland. Questionnaires could be filled in German or English language. Invitations were sent to potential participants via email by the Clinical Trial Centre at the USZ. All study participants provided electronic consent prior to their participation in the health survey. The implementation of the online health survey was approved by the responsible ethics committee of the

canton of Zurich (BASEC-Nr. 2018-01042). Data was collected between 13 April 2022 and 30 May 2022 and a reminder was sent on 03 May 2022 to all participants who had not participated before that date. Data from 142 participants was collected. Data from six individuals was removed from analysis as the survey form was almost entirely incomplete, resulting in a final analysis dataset consisting of 136 individuals. The participation rate was thus 20.4% for those invited via e-mail. While this participation rate may likely be comparable to other surveys, the limited participation may be explained by several factors: (1) we contacted participants by e-mail only, (2) we contacted participants several months after their last healthcare contact, (3) patients of our University Hospital may have a higher baseline morbidity interfering with filling the questionnaires, (4) potential fatal events that may have meanwhile occurred in several patients, (5) expected and known language barriers (the invitations to and the survey were available in German and in English but many of our hospital patients speak e.g. Albanian, Portuguese, French, Italian, Turkish, Ethiopian, or Tamil and other Dravidian languages). We attempted to minimize any selection bias by making the survey as accessible and short as possible, using simple language, and by sending a reminder e-mail to those invited. It cannot be ruled out that some selection has still occurred. However, it is unclear if this would bias the results towards higher (hospital patients with higher morbidity & age included) or lower (younger patients with higher digital literacy included) estimates of post COVID-19 condition. We included all participants that included sufficient data that allowed the assessment of at least part of the outcomes from the survey reported in the manuscript (i.e., current health and prior infection status). For most variables, there was little missingness (<5%) in the questionnaires. [Tables 2](#) and [S3–S5](#) report any missing data.

Data was analysed in R 4.2.0 using descriptive statistics and multivariable logistic regression models adjusted for age and sex.